2014

# Determining Hillslope Diffusion Rates in a Boreal Forest: Quaternary Fluvial Terraces in the Nenana River Valley, Central Alaska Range

Laurel Anne Walker
*University of Kentucky*, laurel.a.walker1@gmail.com

STUDENT AGREEMENT:

I represent that my thesis or dissertation and abstract are my original work. Proper attribution has been given to all outside sources. I understand that I am solely responsible for obtaining any needed copyright permissions. I have obtained needed written permission statement(s) from the owner(s) of each third-party copyrighted matter to be included in my work, allowing electronic distribution (if such use is not permitted by the fair use doctrine) which will be submitted to UKnowledge as Additional File.

I hereby grant to The University of Kentucky and its agents the irrevocable, non-exclusive, and royalty-free license to archive and make accessible my work in whole or in part in all forms of media, now or hereafter known. I agree that the document mentioned above may be made available immediately for worldwide access unless an embargo applies.

I retain all other ownership rights to the copyright of my work. I also retain the right to use in future works (such as articles or books) all or part of my work. I understand that I am free to register the copyright to my work.

REVIEW, APPROVAL AND ACCEPTANCE

The document mentioned above has been reviewed and accepted by the student's advisor, on behalf of the advisory committee, and by the Director of Graduate Studies (DGS), on behalf of the program; we verify that this is the final, approved version of the student's thesis including all changes required by the advisory committee. The undersigned agree to abide by the statements above.

Laurel Anne Walker, Student

Dr. Sean P. Bemis, Major Professor

Dr. Edward W. Woolery, Director of Graduate Studies

# DETERMINING HILLSLOPE DIFFUSION RATES IN A BOREAL FOREST: QUATERNARY FLUVIAL TERRACES IN THE NENANA RIVER VALLEY, CENTRAL ALASKA RANGE

---

THESIS

---

A thesis submitted in partial fulfillment of the
Requirements for the degree of Master of Science in the
College of Arts and Sciences
At the University of Kentucky

By

Laurel Anne Walker

Director: Dr. Sean P. Bemis, Assistant Professor of Earth and Environmental Sciences

Lexington, Kentucky

2014

ABSTRACT OF THESIS

DETERMINING HILLSLOPE DIFFUSION RATES IN A BOREAL FOREST:
QUATERNARY FLUVIAL TERRACES IN THE NENANA RIVER VALLEY, CENTRAL ALASKA RANGE

The subarctic boreal forest biome is predicted to experience higher magnitudes of warming than other biomes due to climate change. The effects of this warming will be pronounced in areas underlain by discontinuous permafrost where melting permafrost and distinct changes in vegetation patterns are expected. To better understand rates of hillslope diffusion in the boreal forest I have used a geomorphic process modeling approach, using data from a sequence of Quaternary fluvial terraces located in the Nenana River valley of central Alaska. I hypothesized that diffusion rates here would be slower when compared to the mid-latitudes, and faster on north versus south-facing slopes. Calculated diffusion rates do support the hypothesis as they fall on the lower end of the global spectrum of documented hillslope diffusion rates. However, a significant difference in diffusion rates is not seen between the predominantly northeast and southwest facing slopes used in this study.

KEYWORDS: Alaska Range; Nenana River Valley; Boreal Forest; Hillslope Diffusion; Optically Stimulated Quartz Luminescence

Laurel Anne Walker

April 24, 2014

DETERMINING HILLSLOPE DIFFUSION RATES IN A BOREAL FOREST:
QUATERNARY FLUVIAL TERRACES IN THE NENANA RIVER VALLEY, CENTRAL ALASKA RANGE

By

Laurel Anne Walker

Sean P. Bemis, Ph.D.
*Director of Thesis*

Edward Woolery
*Director of Graduate Studies*

April 24, 2014

ACKNOWLEDGEMENTS

I would like to thank Dr. Sean Bemis for his endless support and help in both the field and office. I would like to thank Josh DeVore for his help in field work, and OSL processing, as well as the entire Neotectonics Research Team from the University of Kentucky for their help in the field. I would also like to thank Shannon Mahan for her hard work in the USGS OSL lab as well as her contributions to chapter two of this thesis. I would also like to thank the University of Kentucky Department of Earth and Environmental Sciences, Alaska Geological Society, and Graduate Women in Science Beta Chi Chapter for research support.

In addition, I would to thank my parents and all of my siblings; Jeff, Kathy, Peter, Mary Claire, Patrick, Forrest, Rachel and Hannah for their continued support, and companionship in outdoor adventures; my father for instilling in me a love for geology and teaching, and my mother for giving me her curious and adventurous nature.

TABLE OF CONTENTS

LIST OF TABLES

LIST OF FIGURES

# Chapter One:

# Hillslope diffusion rates and controls on landscape evolution in the boreal forest, central Alaska

## 1.1 Introduction

Landscape evolution in the boreal forest is controlled by several key environmental and topographic factors including aspect, permafrost, vegetation, and soil moisture. Each of these factors are influenced by differences in solar insolation, either directly (e.g. aspect) or indirectly (e.g. vegetation). In the boreal forest biome low sun angles accentuate the effect of topography on environmental factors (Bonan, 1989; Chapin et al., 2006) producing cold, wet, gentler northerly facing slopes (Chapin et al., 2006), and warm, well-drained, steeper southerly facing slopes. The boreal forest is defined by the presence of discontinuous permafrost making it a fragile environment where organisms are adapted to a specific regime. Therefore, small changes in temperature can cause large changes in permafrost due to melting (Anthony et al., 2012). Rowland et al. (2010), demonstrates that subsequent changes in the permafrost regime can have significant effects on erosion, vegetation, and other surface processes.

The goals of this study were to determine hillslope diffusion rates for a boreal forest, second to answer the question of if and how these rates might change with time and climate, and third to see if aspect significantly affects hillslope diffusion. To understand the geomorphic processes that govern hillslope diffusion in this environment I chose to use a sequence of fluvial terrace risers in the Nenana River

valley of central Alaska (Figures 1.1, 1.2). The terrace risers I chose provide sequentially occurring landforms whose original shape can be reliably inferred and each one provides a snapshot of landscape evolution over a discrete period of time, corresponding to three key glacial advances; Carlo (14-18 ka, marine isotope stage (MIS) 2), Riley Creek (22-30 ka, MIS 2), and Healy (ca. 60 ka, MIS 4) (Dortch et al., 2010). This sequence of terraces is appropriate for this study because they are relatively well-preserved and I was able to choose the surfaces which appeared to be predominantly acted upon by diffusive processes not erosive fluvial/alluvial processes, post-abandonment. I examined the terrace risers to look for trends in diffusive behavior, compare risers of different ages and aspects, and analyze their overall evolutionary nature, similar to other studies such as Hsu and Pelletier (2004) and Hanks (2000). After initial first-order observations, elevation and across slope profile data was extracted to analyze and quantify hillslope diffusion behavior. These data were then used to solve for the diffusivity constant "*k*," which is an amalgamation of the suite of processes that acts on a hillslope in a given environment. These processes include bioturbation by plants and animals, effects of permafrost and periglacial processes, climate, and solar radiation. Hillslope diffusion rates in central Alaska were compared both to each other, as well as to mid-latitude environments, in terms of aspect versus hillslope diffusion rates. The hillslope diffusion rates resulting from this study were also compared to higher resolution elevation data having partial coverage in the field area, to assess any bias introduced by the lower resolution data. The results of this work are significant not only because they add to our understanding of the interplay between geomorphic processes and climate cycles in

central Alaska, but because they also present a baseline for future studies of landscape evolution in boreal forest environments not previously available. Landscape evolution and diffusion rates have not been closely studied or reported for the boreal forest region.

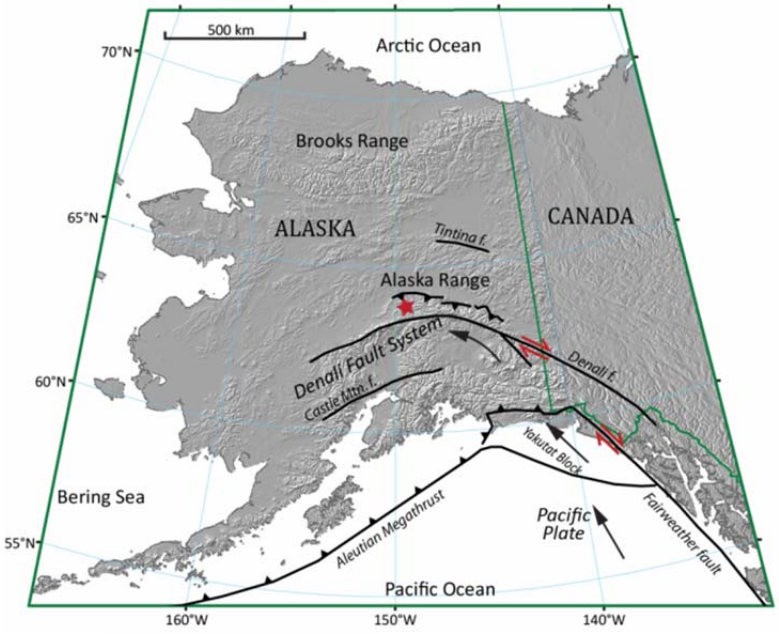


**Figure 1.1 Regional map of Alaska with major faults labeled.** The Nenana River Valley is denoted by the red star. My study site is situated withn the northern foothills of the Alaska Range, where active deformation of the northern Alaska Range thrust system has produced an extensive suite of glaciofluvial terraces along major drainages (Bemis et al., 2012). Adapted from Bemis (2010).

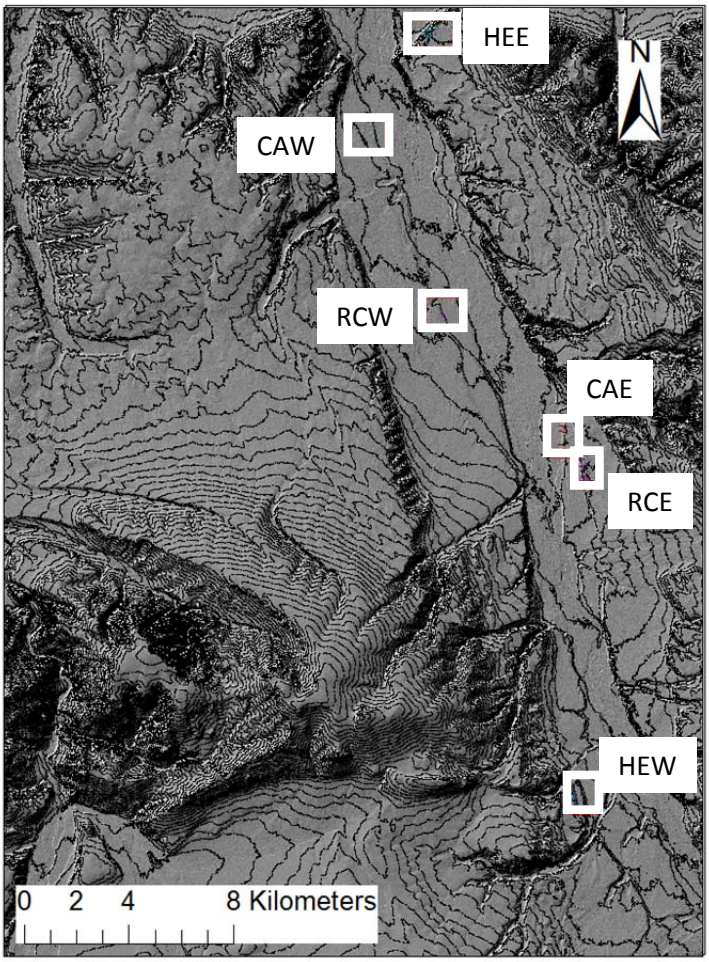


**Figure 1.2: Study Locations.** This figure shows the general study area in the Nenana River valley of the central Alaska Range (red star on Figure1.1). White boxes indicate portions of the terrace risers from which topographic profiles were extracted. 20 m contour interval. Site nomenclature: Healy West and East = HEW and HEE, Riley Creek West and East = RCW and RCE, Carlo West and East = CAW and CAE. At each site, six profiles were taken and numbered 1-6 (i.e CAW 1, CAW2, etc; see Appendix A). At site CAW the same six profiles were also extracted from LiDAR data numbered CAWL1, CAWL2, CAWL3, CAWL4, CAWL5, CAWL6.

## 1.2 Study Area: Regional Setting and Characteristics

*1.2*.1 *Setting*

The east-central Alaska Range is part of a 1000 km long, arcuate mountain belt which extends from the Canadian border to the Alaska Peninsula in southwest Alaska (Figure 1.1). The active tectonics of this area are shaped in part by the accretion and flat-slab subduction of the Yakutat terrane and Pacific plate under the North American plate in southeastern Alaska (Eberhart-Phillips et al., 2006). The Denali-Totschunda fault system accommodates the transfer of strain from the southern Alaska plate margin far into central Alaska. The Alaska Range occurs as a transpressional mountain belt running parallel with the Denali fault as it arcs across south-central Alaska. The fluvial terraces of the Nenana River valley (Figure 1.1) result from episodic climatic changes throughout the Quaternary superimposed upon the long-term uplift of the Alaska Range (Bemis, 2010).

This pattern of aggradation and floodplain formation associated with glacial advances and subsequent terrace formation (floodplain abandonment), resulting from downcutting following glacial retreat, is a pattern observed in tectonically active mountain ranges around the world (Molnar et al., 1994).The most extensively- sequence of terraces and geomorphic features in Alaska are found in the Nenana River valley. The Quaternary glacial history of the region was originally documented by Wahrhaftig (1958) with several modifications since by Ten Brink and Waythomas (1985),Thorson (1985),

Bemis and Wallace (2007), (Dortch et al., 2010) and Bemis (2010). Within this sequence, the oldest surface represents the top of the Plio-Pleistocene Nenana Gravel (a coarse-grained alluvial sequence that filled the former Alaska Range foreland basin) which records the initial uplift of the northern Alaska Range resulting from thrust fault propagation during the Early Pleistocene (Bemis et al., 2012). Glacial erratics in the uppermost stratigraphy of the Nenana Gravel have been noted by several researchers and may support the early Pleistocene age assigned to this surface.

The Alaska Range is a significant orographic boundary acting to inhibit the amount of precipitation in interior Alaska derived from the Gulf of Alaska. Because of this, Pleistocene summers in central Alaska were relatively warmer and drier than other areas of Alaska and kept the region ice-free during Quaternary glacial advances, except for piedmont glaciers in north-flowing drainages along the northern side of the Alaska Range (Wahrhaftig, 1958) and scattered alpine glaciers associated with local high elevations within the Yukon-Tanana Upland (Briner and Kaufman, 2008).

### *1.2.2 Formation of the terrace sequence*

The formation of the Nenana River valley fluvial terraces represents a complex sequence of aggradational and degradational processes, but as landforms they are strath terraces. The alternating aggradational and degradational behavior that this terrace sequence represents is related to the relationship between supply and transport (stream power), such that an increase in stream power causes an increase in energy available to overcome friction and causes degradational behavior, and a decrease in

stream power has the opposite effect. This pattern of aggradation and incision in the Nenana River valley is the product of multiple glacial/interglacial cycles which produced shifts in sediment load and caliber and discharge. The superposition of this alternating aggradation and incision upon the Quaternary uplift of the northern foothills of the Alaska Range produced an extensive suite of progressively uplifted and deformed fluvial terraces.

The terrace sequence of the Nenana River valley shows a typical Quaternary glacial sequence with successive glacial advances having termini progressively farther up the valley. The oldest geomorphic surface is a broad regional aggradational plain that represents the top of the Plio-Pleistocene Nenana Gravel. More recently Bemis (2010) introduced a nomenclature for the terrace sequence (Q1-Q7), where Q1 corresponds to the Nenana Gravel, and Q2-Q7 represents progressively younger glacial advances (Table 1.1). Current geological age constraints (Table 1.1) are derived from terrestrial cosmogenic nuclide dating (e.g., Dortch et al., 2006), optically stimulated luminescence (OSL) (e.g., Dortch et al., 2010) and regional or global correlations (e.g. Bemis, 2010).

TABLE 1.1. AGE CONSTRAINTS AND CORRELATIONS

| Surface Name | Regional Correlation | Age Constraints | MIS |
|---|---|---|---|
| Modern river level | n/a | Modern | n//a |
| Q7 | Carlo | ~14-16 ka | MIS 2 |
| Q6 | Riley Creek | ~20-30 ka | MIS 2 |
| Q5 | Healy | ~60 ka | MIS 4 |
| Q4 | Lignite Creek | ~130-200 ka | MIS 6 |
| Q3 | ??? | n/d | n/a |
| Q2 | Browne | ~1.15 Ma | n/a |
| Tn (Q1) | Nenana Gravel | >1.0 Ma<br>2.0-2.6 Ma | n/a |

*1.2.3 Changes in vegetation patterns throughout the Quaternary*

Much of the subarctic region now covered by the boreal forest has not always been forested. Even though much of this region in Alaska remained ice-free throughout the Quaternary, major climatic fluctuations still caused forested landscapes to repeatedly appear (during interglacial cycles) and disappear (during glacial cycles) (Chapin et al., 2006). Not only did forested landscapes in the Nenana River valley disappear during glacial cycles but vegetation in general, including shrubs and groundcover, largely disappeared as well due to increased wind speed, stream power, and glaciation. This lack of vegetation during glacial periods likely created less stable slopes relative to interglacial periods, subsequently changing their downslope transport behavior. Downslope sediment transport is divided into two different categories based on the dominant controlling factor; loosening limited and transport limited. Loosening-limited slopes are limited by the supply of material up slope (e.g. non-vegetated, bare-rock) and transport-limited slopes are limited by the transport of sediment away from the base of a slope (e.g. vegetated, soil-mantled) (Nash, 1984). The most recent glacial period was dominated by a treeless landscape, until ~13,000 BP, when the boreal forest re-emerged as a widespread ecosystem (Chapin et al., 2006).

During the Holocene, central Alaska was dominated by three distinct forest types: open woodlands dominated by broadleaf species in the early Holocene (13,000-10,000 BP); white and black spruce during the mid-Holocene (10,000-5,000 BP); and

black spruce during the late Holocene (5,000 BP to present) (Chapin et al., 2006).These three forest types show two major transitions occurring during the Holocene, one from broadleaf open woodlands to white spruce and one from white spruce to black spruce (Chapin et al., 2006).

Modern vegetation of central Alaska at lower elevations (<460 m) mainly consists of species typical of the northern boreal forest (Viereck, 2010). The dominant trees and shrubs are split into two landscape positions within the boreal forest biome (Muhs, 2001), well-drained upland sites and poorly drained lowland sites. On the former sites, white spruce, paper birch, and aspen are found with an understory of mosses, currants, Labrador tea, and blueberry. In drier areas the underbrush may contain more grasses and open forests can have willow and alder. Poorly drained lowland sites, especially if they are underlain by shallow permafrost, are characterized by the occurrence of black spruce. The understory in these poorly drained areas is mainly willow, Labrador tea, shrub birch, blueberry, sedge, and mosses. The treeline elevation is usually at about 900-1,000 meters elevation, except on north-facing slopes which often have a slightly lower tree line and the forest grades into moist tundra with dwarf birch, willow, and herbaceous species. The factors that control the boreal forest environment are complex, and include the presence of permafrost, length of the growing season, and temperature. The northern limit of the spruce forest is defined by snow cover, nutrient-poor unstable soils, and discontinuous permafrost (Larsen, 1980) and in Alaska specifically, the northern limit of the boreal forest is marked by the Brooks Range (Muhs, 2001). Some boreal forest in Alaska and Canada contains small pockets of

locally drier conditions on steep south facing slopes which contain steppe vegetation, so boreal forest is not necessarily the sole biome in this region (Edwards and Armbruster, 1989). Sometimes these same enclaves are found in areas where rain shadow effects and katabatic winds combine and produce locally dry conditions. However, these steppe pockets were not observed in the immediate study area.

## 1.3. Methods

### *1.3.1 Scientific Basis*

The extraction of sediment transport processes and rates from a landscape requires a process-based, equation that can accommodate the complex feedbacks within the system and that can be rearranged to obtain the desired observation from the available data. This model also must be appropriate for the particular geomorphic and incorporate sediment transport processes acting within this specific environment. This means that the equation must not only be appropriate to the boreal forest study region but must also be applicable, specifically, to fluvial terrace riser landforms. The original underlying ideas behind diffusive sediment flux state that elevation (*z)* is viewed as a function of the geometrical and time variables (*x, y, t)* (Culling, 1960). Therefore, material flow takes place at a rate proportional to slope gradient. Culling (1960) first applied this equation to flowing streams and valley slopes. Building on Culling's stream flow and valley slope applications, Nash (1984) introduced two main types of degradation patterns that could be applied to fluvial terrace risers and quantified using a sediment flux equation. Transport-limited slopes become more convex with time, are

covered with soil, and produce more loose debris than the slope is capable of transporting. Alternatively, retreating slopes degrade with little or no change in gradient, are generally bare of debris, and are often termed weathering-limited since debris is removed just as quickly as it is loosened from the surface. For example, a bare, bedrock scarp presents a weathering-limited condition and would represent a retreating scarp.

The nonlinear sediment flux equation takes into account diffusive processes such as tree throw, rain splash and solifluction, as well as slope failure processes such as slumping, and gelifluction. Soil-mantled hillslopes follow a nonlinear diffusion relationship because curvature does not remain constant throughout the length of the slope; rather it approaches zero as the slope steepens towards a limiting angle, the inflection point of the slope (Roering et al., 1999) (Figure 1.3). Therefore, investigating diffusive processes on Quaternary soil mantled fluvial terrace risers in the Nenana River valley requires implementation of the nonlinear diffusion model.

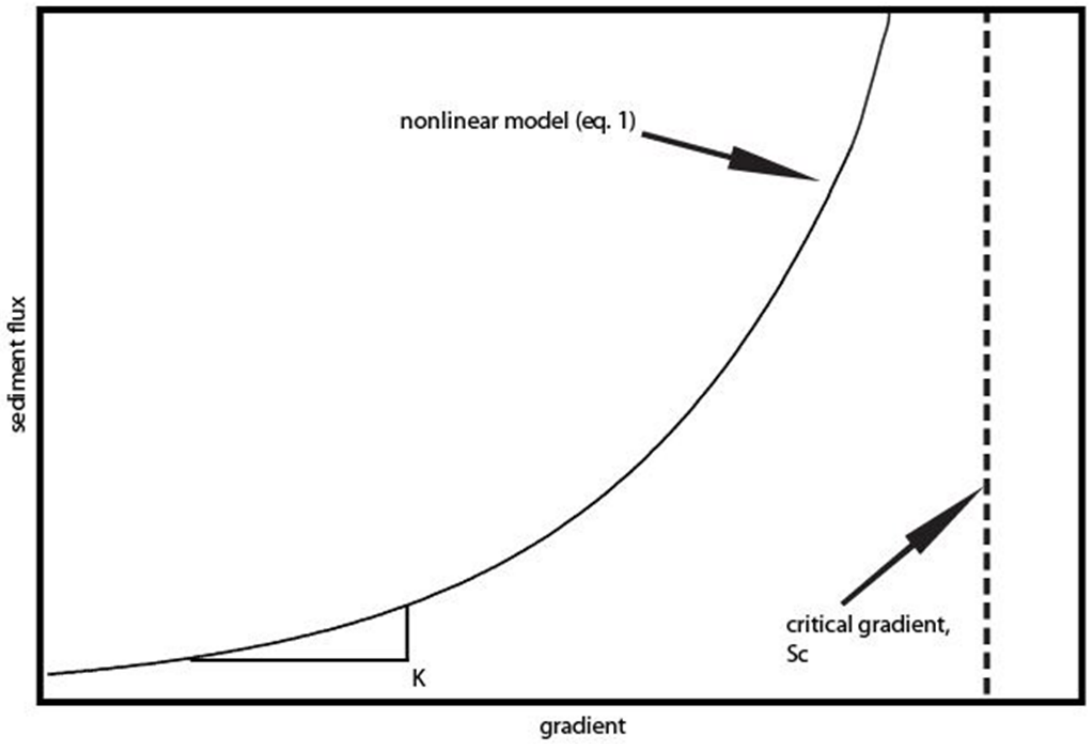


**Figure 1.3 Theoretical relationship between sediment flux and gradient** The curve represents the nonlinear transport law (equation 1), the critical gradient (dotted line), is the gradient at which flux becomes infinite for the nonlinear transport law.

*1.3.2 Nonlinear Hillslope Behavior*

For Gilbert's (1909) proposal of a linear relation between hillslope diffusion and gradient to be true, hillslope curvature must be constant, which is only the case with an increasingly convex slope. More recent work has proposed that diffusion rates increase in a nonlinear manner as the slope steepens (Clarke and Burbank, 2010; Hsu and Pelletier, 2004; Roering et al., 1999). Roering et al. (1999) present the following

equation to model the nonlinear relationship between sediment flux, $q_s$, and hillslope gradient (equation 1):

(1)

$$q_s = \frac{k \tan \theta}{\left(1 - \left(\frac{\tan \theta}{S_c}\right)^2\right)}$$

Where $k$ is diffusivity ($m^2$/year) and varies based on climate, vegetation, geology and many other factors, $\theta$ is hillslope gradient, and $S_C$ is the critical hillslope gradient for mass-movement. As the critical hillslope gradient is reached, the rate of sediment flux reaches infinity (meaning that gravity is the only factor controlling sediment movement after this point). The critical hillslope gradient is a function of cohesion, internal friction of the soil, soil moisture content, indirectly through vegetation and is comparable to the angle of repose. I have re-arranged the equation in order to solve for $k$ (eq. 2 below) using elevation and length of profile data extracted from our site (inverse modeling) and used an average of between 30° and 40° (0.71) for my $S_c$ value based on the angle of a relatively young, vegetated terrace riser (Figure 1.4).

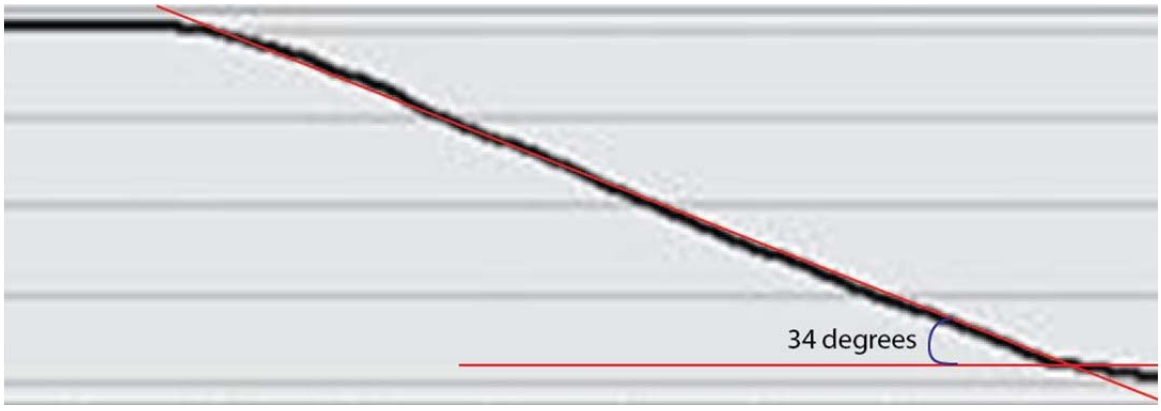


**Figure 1.4: Illustration of $S_c$ constraint.** This riser is considered representative of $S_c$ because the profile is relatively linear; there is very little curvature at the top and

bottom, suggesting minimal diffusive processes have acted on it. Further, satellite images show that it is vegetated and stabilized such that mass-wasting processes have ceased. The maximum gradient of this terrace riser (34°) is the $S_c$ value in this study.

*1.3.3 Solving for k*

Solving equation 1 for k produces equation 2:

(2)

$$k = \frac{(q_s)\left(1 - \left(\frac{\tan\theta}{S_c}\right)^2\right)}{\tan\theta}$$

Where *k* is diffusivity ($m^2/t$), $\theta$ is hillslope gradient, and $S_C$ is the critical hillslope gradient, and $q_s$ is sediment flux ($m^2/t$). To solve equation 2 I need to determine the area of sediment moved and divide it by the age of the landform (sediment flux), the maximum slope gradient (point of zero curvature), and insert the appropriate $S_c$ value. In order to calculate *k* values, I used elevation and slope length data from six topographic slope profiles for each age on each side of the Nenana River *k* (Figure 1.4a-1.6b). I calculated *k* for each profile using a critical hillslope ($S_c$) value of 0.71, which corresponds to a 34° slope angle. The critical hillslope angle is similar to the angle of repose and, based on a relatively young, vegetated terrace riser as a model (Figure 1.3), is approximately 34° for this region. The age factor in the equation is inferred from the tread at the base of the riser, because the riser would be cut while the terrace below was an active floodplain. Following incision and abandonment of that floodplain, the

terrace riser becomes isolated and once stabilized from mass-wasting processes, ideally begins to erode through diffusive processes.

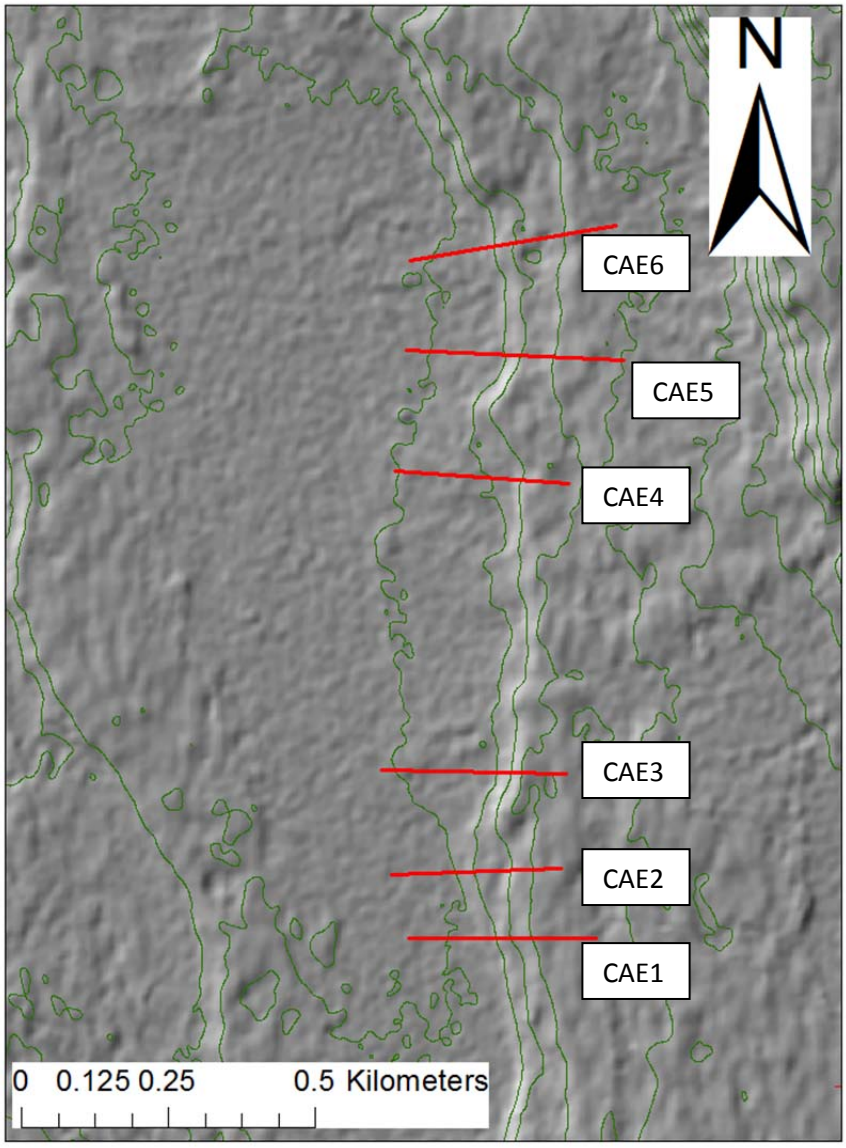


**Figure 1.5a Locations of topographic profiles across Carlo-aged terrace risers (east side of the Nenana River valley).** These profiles were extracted from IfSAR DTM (bare-earth DEMs) with a horizontal accuracy of 12.2 m, contour interval is 5 m, and the hillshade illumination orientation is from 315°. Source: http://ifsar.gina.alaska.edu/

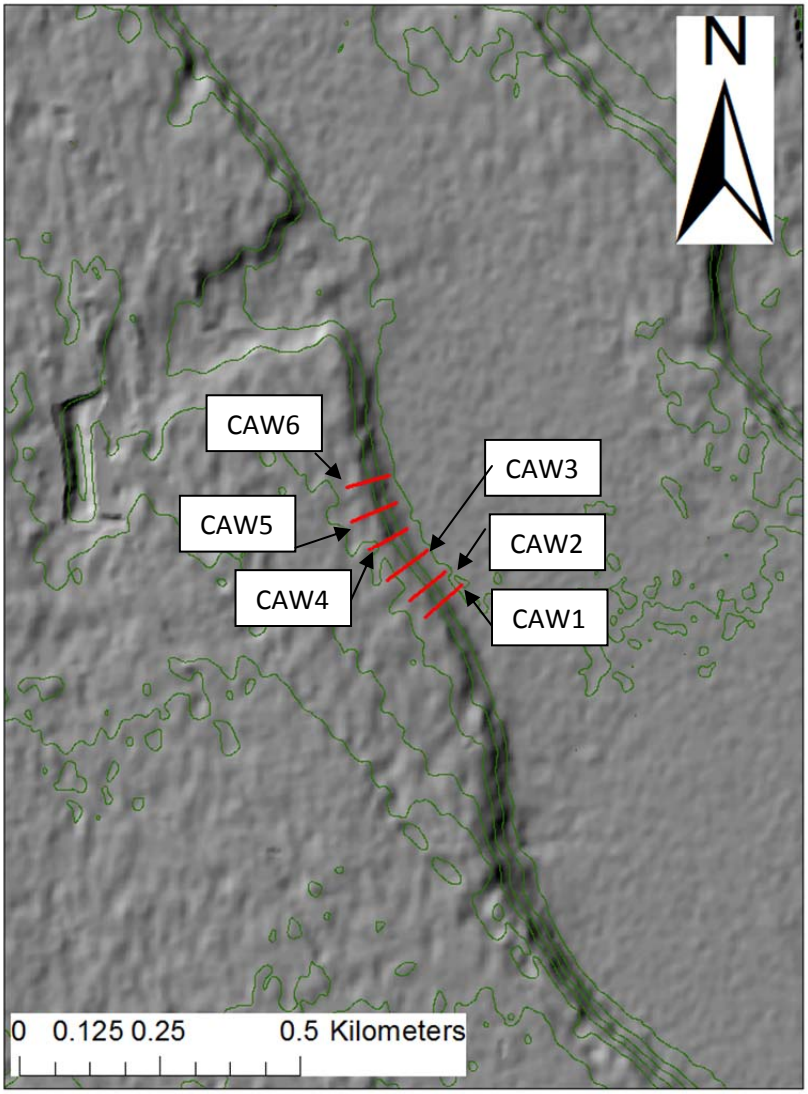


**Figure 1.5b Locations of topographic profiles across Carlo-aged terrace risers (west side of the Nenan River valley.** These profiles were extracted from IfSAR DTM (bare-earth DEMs) with a horizontal accuracy of 12.2 m, contour interval is 5 m, and the hillshade illumination orientation is from 315°. Source: http://ifsar.gina.alaska.edu/

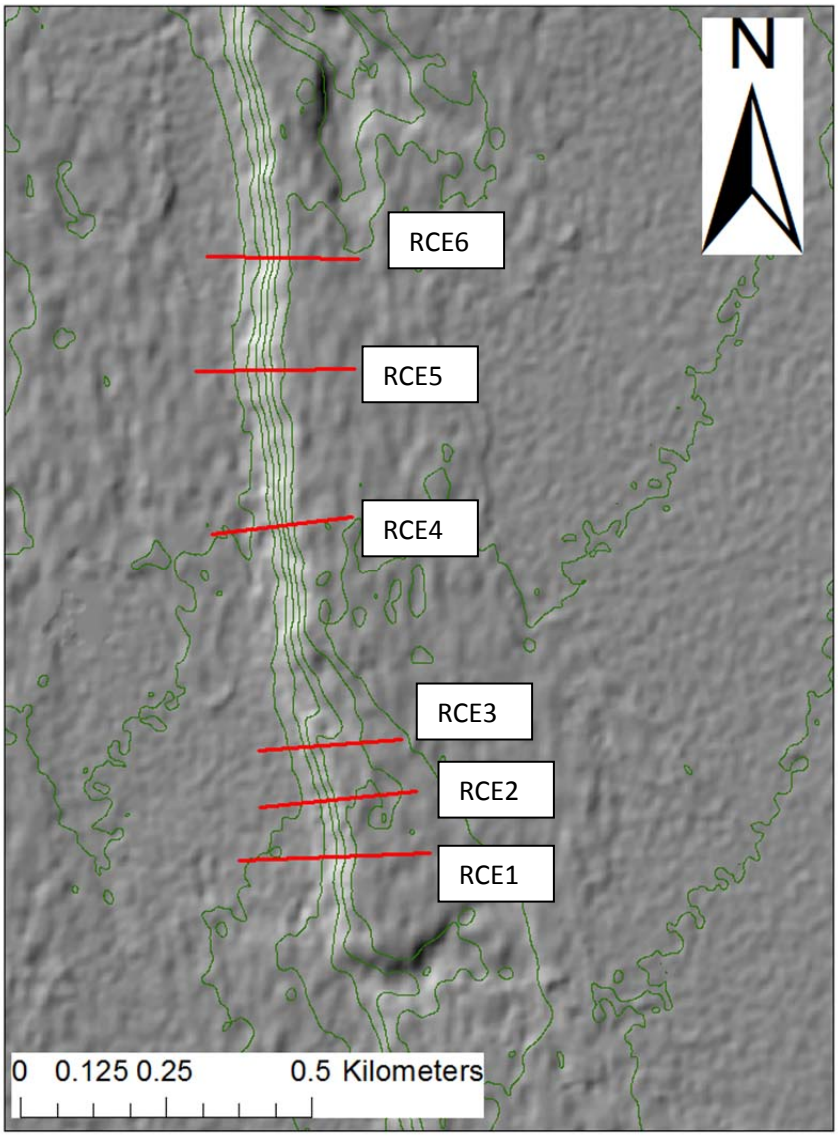


**Figure 1.6a Locations of topographic profiles across Riley Creek-aged terrace risers (east side of the Nenana River valley).** These profiles were extracted from IfSAR DTM (bare-earth DEMs) with a horizontal accuracy of 12.2 m, contour interval is 5 m, and the hillshade illumination orientation is from 315°. Source: http://ifsar.gina.alaska.edu/

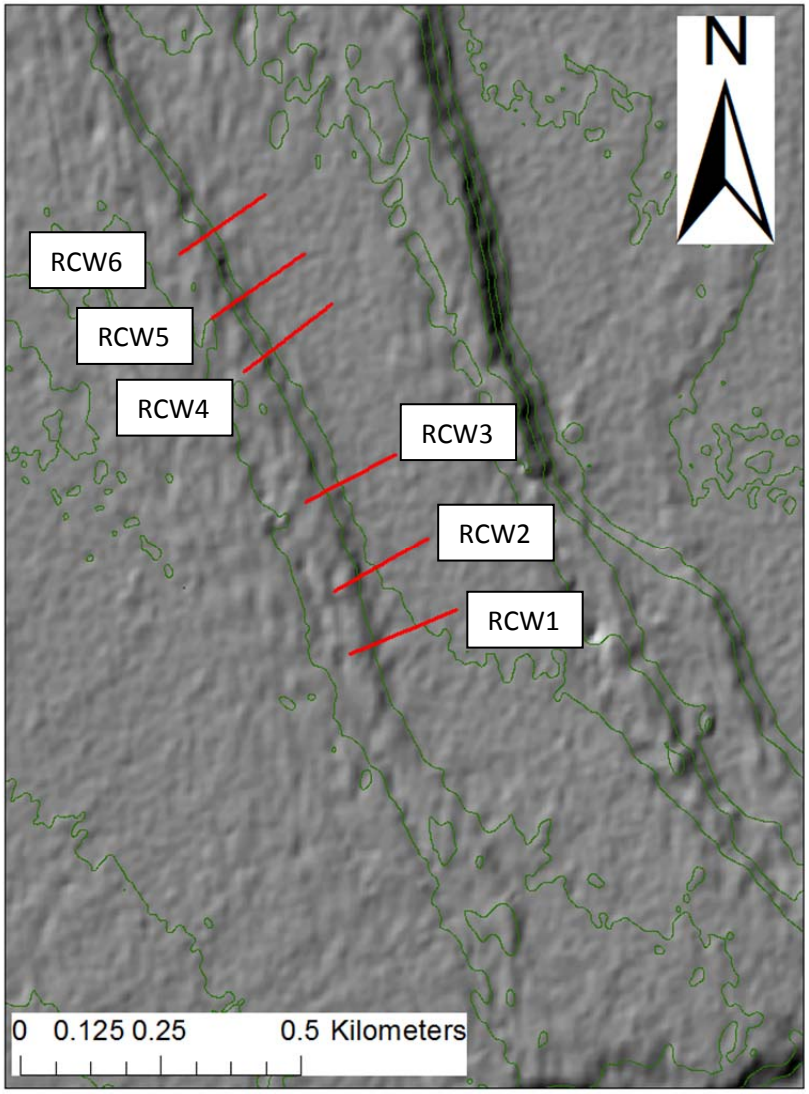


**Figure 1.6b Location of topgraphic profiles across Riley Creek-aged terrace risers (west side of the Nenana River valley).** These profiles were extracted from IfSAR DTM (bare-earth DEMs) with a horizontal accuracy of 12.2 m, contour interval is 5 m, and the hillshadeillumiantion orientation is from 315°. Source: http://ifsar.gina.alaska.edu/

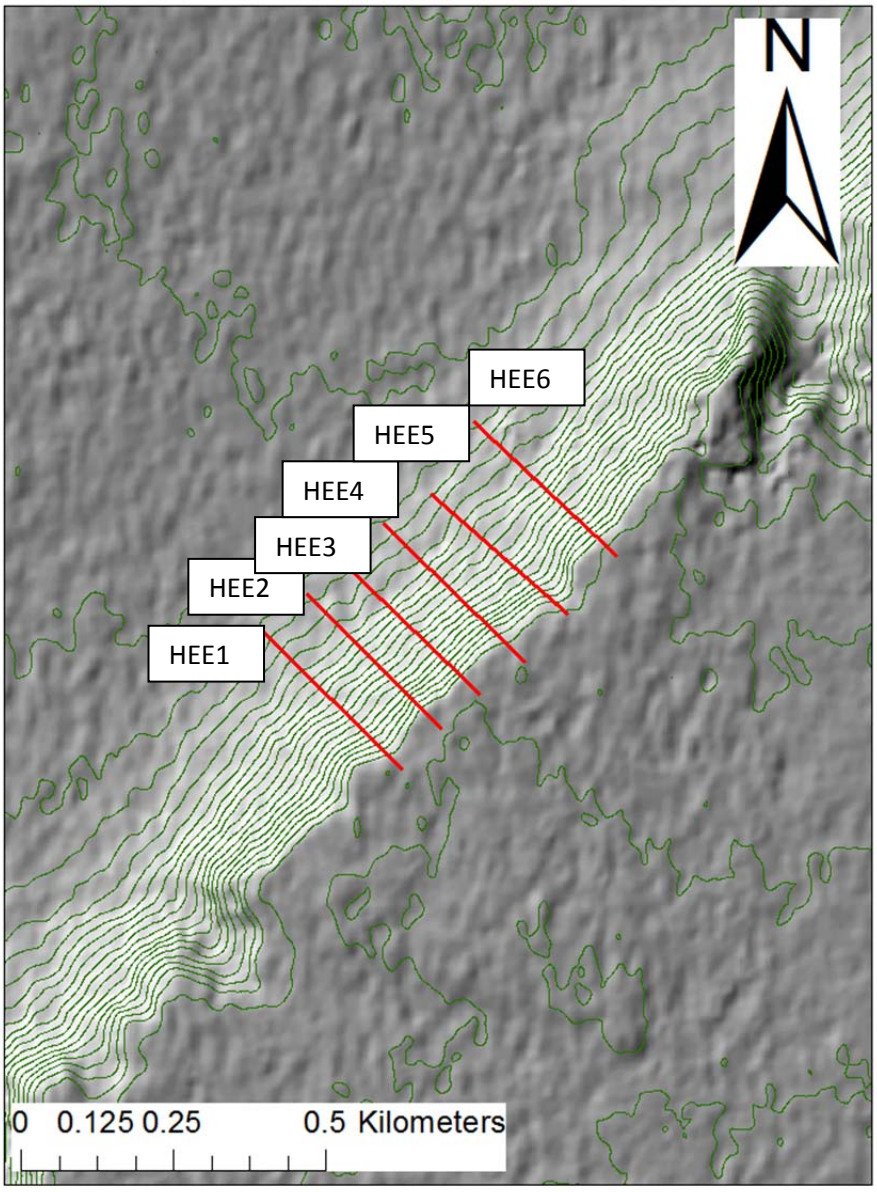


**Figure 1.7a Locations of topographic profiles across Healy-aged terrace risers (east side of the Nenana River valley.** These profiles were extracted from IfSAR DTM (bare-earth DEMs) with a horizontal accuracy of 12.2 meters. The scale bar is 0.5 km, contour interval is 5 meters, and the hillshade illumination orientation is from 315°. Source:

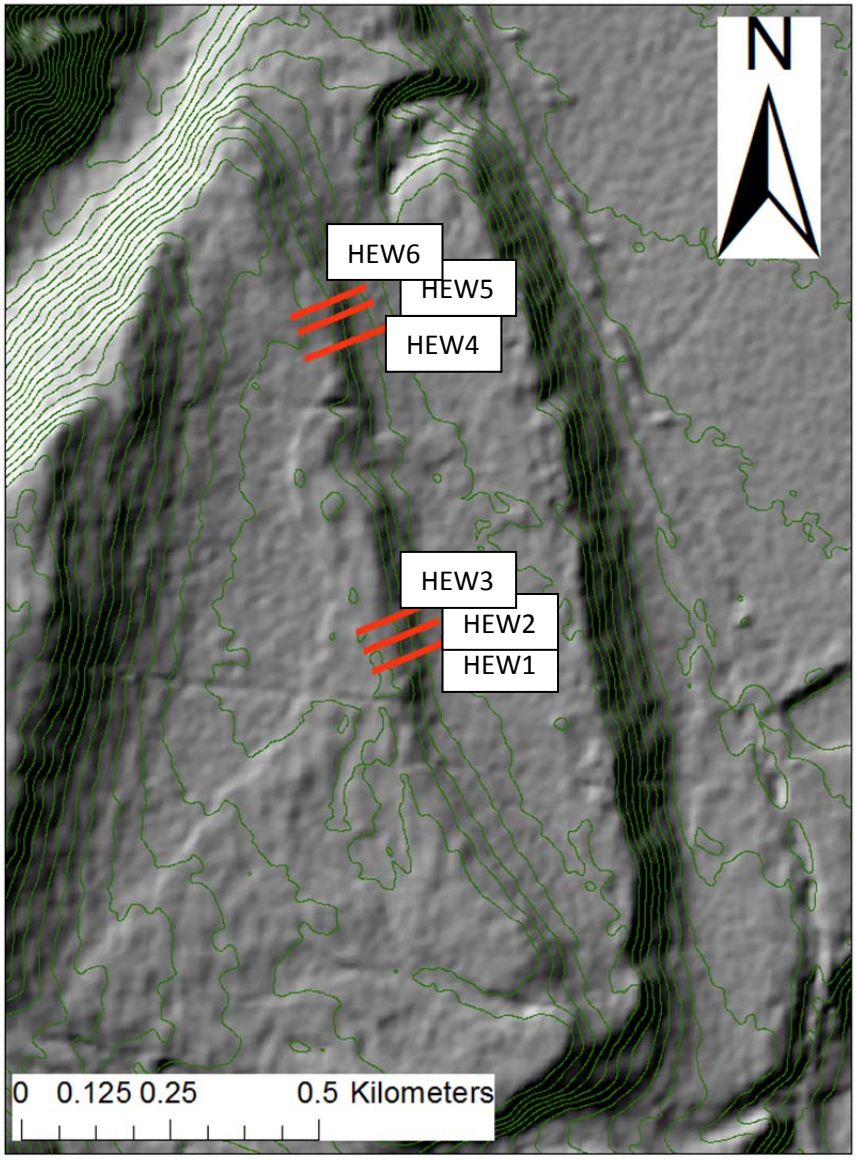


**Figure 1.7b Locations of profiles across Healy-aged terrace risers (west side of the Nenana River valley).** These profiles were extracted from IfSAR DTM (bare-earth DEMs) with a horizontal accuracy of 12.2 meters. The scale bar is 0.5 km, contour interval is 5 meters, and the hillshade illumination orientation is from 315°. Source: http://ifsar.gina.alaska.edu/

A third order polynomial provides a function that closely approximates the natural topographic profile data for the terrace risers. This function was fit to each individual set

of profile data and the point of 0 curvature (midpoint and location of maximum gradient) on the slope was calculated. I then calculated the area of sediment above the midpoint by calculating the area under the line from a – c (integral of g(x)), the area under the curve (A) from a – c (integral of f(x)) and the area of the triangle (B) and subtracted them from one another to get C (Figure 1.5, equation 3).

(3)

$$\int_a^c g(x) - \int_a^c f(x) - \frac{1}{2}\, bh$$

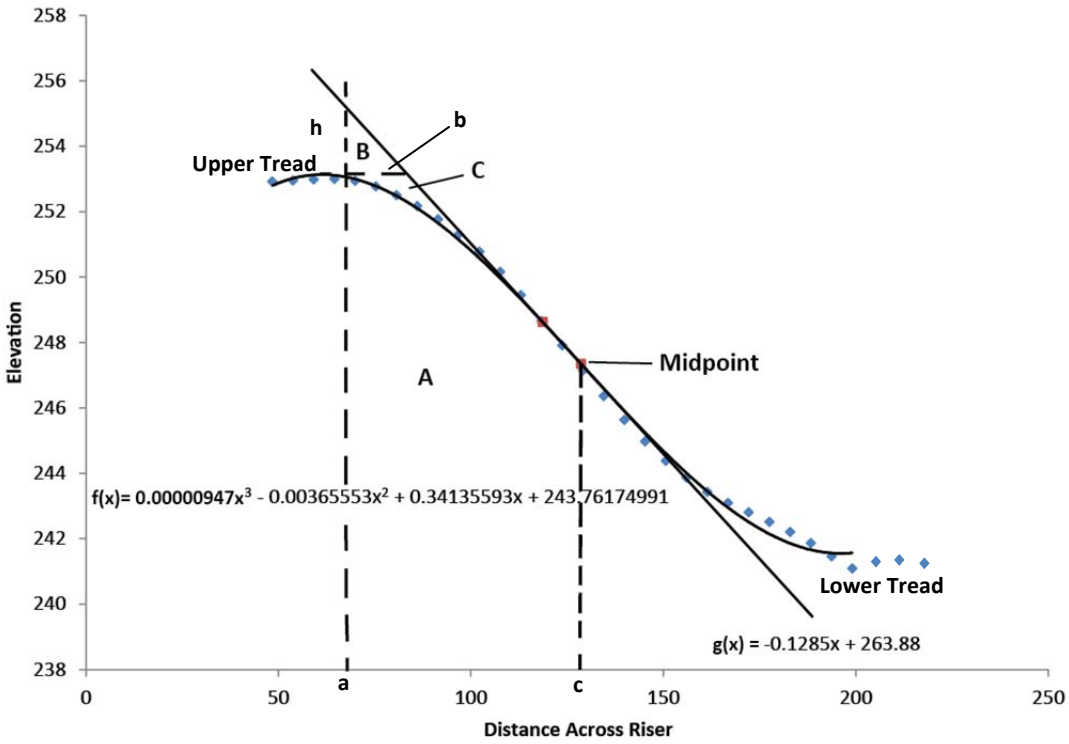


**Figure 1.8: Example slope profile and data extraction method.** This figure shows elevation versus length along riser points taken from a Riley Creek-aged terrace on the west side of the Nenana River (blue dots). A third-order polynomial (f(x); black curved line) provides a close fit to the data. Solving the second derivative of this line for x yields

the midpoint (point of zero curvature on the riser (see Figure 1.7). The area under the straight line, area of box "a" and triangle "b" were determined and subtracted from one another to get the area of "c" which is equal to the amount of sediment moved and used in the calculation of $q_s$ in my calculation of k.

I calculated *k* and the propagated error for each respective glaciation and cardinal direction. Error in age constraints is the main source of uncertainty in calculations. I quantified this error by multiplying calculated *k* value by a 10-15% age range based on the variation in each of the ages (for example 5 ky of error if an age ranged from 20-30 ky) and dividing this number by the average age (in our example 25 ka). The following equation calculates the error in the *k* data (equation 4):

(4)

$$\Delta k = k\left(\frac{\Delta t}{t}\right)$$

Where $\Delta k$ = error, $\Delta t$ = error in age, $t$ = age, and $k$ = diffusivity constant. After calculating *k* for each profile drawn I plotted average k values versus landform age (Figure 1.10). I included error on ages (Table 1.2) as well as calculated error on *k* values for each of the three different aged (Carlo, Riley Creek, and Healy).

### *1.3.5 Testing Accuracy of IfSAR DTMs against LiDAR DTMs*

LiDAR, which stands for light detection and ranging, measures ranges (variable distances) to the Earth using light in the form of a pulsed laser (Slatton and Carter, 2008). Then these light pulses are combined with position and orientation data to generate a three-dimensional model of the Earth. When the laser ranges, positions, orientations, scan angles, and calibration angles are combined the result is a detailed,

dense group of elevation points referred to as a “point-cloud” (Slatton and Carter, 2008)**.** Each of the points in the point cloud has a three-dimensional spatial coordinate (latitude, longitude, and height), which corresponds to the particular point on the surface where the laser reflected off of. These point clouds are then used to generate a variety of geospatial products; including DEMs, canopy models, building models, and contours. DEMs are split into two categories, digital surface, and digital terrain models (DSMs and DTMs). DSMs are an accurate representation of the Earth’s surface and its features, but for many applications, such as landscape evolution analysis, where only the bare earth is desired, a DTM is required. For this study I used DTMs, which are DSMs that have been further processed to filter out vegetation and other surface features.

Synthetic aperture radar (SAR), determines the amount of scattered energy returned to an antenna as well as its range and position. If two SAR images are combined the technique is referred to as interferometric SAR (IfSAR) and will generate a DEM. The elevation of any single pixel (resolution cell, 5 m sample distance) is the result of a combined signal scatterer located within the resolution cell (sample area) (Dowman, 2004). The measured elevation for any DSM model (resolution cell) is made up of a combined signal scatter from all objects and features located within this sample area. For example, if trees are near a road then both the trees and road (bare earth) will contribute to the elevation model measured for any one DSM sample. IfSAR is advantageous because it is significantly cheaper to acquire than LiDAR, making it suitable for relatively larger areas of study.

LiDAR coverage for Alaska is mainly limited to the highway corridors, which only encompasses a narrow swath through the Nenana River valley. DEMs derived from this LiDAR are high resolution 1 m cell size and are publicly available online at http://maps.dggs.alaska.gov/lidar. On the other hand, much of the state of Alaska is covered by IfSAR, including my entire study area. The Alaska IfSAR DEM data are available online at http://ifsar.gina.alaska.edu/. The elevation models derived from this IfSAR data have a 2.5 m cell size.

To test the accuracy of *k* values derived from the lower resolution but more spatially extensive IfSAR DEMs, I performed a duplicate analysis using LiDAR DEMs for a portion of the region with coverage by both data sets. The higher resolution of the LiDAR data should produce lower diffusivity values because the lower spatial resolution IfSAR imparts a smoothing of the riser crest that would mimic a higher amount of downslope sediment transport and lead to a higher diffusivity value. Therefore, if a persistent offset exits in terms of the derived diffusivity values, then a correction factor for diffusivity values between these DEM datasets may allow for the use of a more widespread IfSAR data for landscape evolution studies throughout portions of Alaska (Figures 1.9, and 1.10). To test the accuracy of the IfSAR data against LiDAR data I extracted a set of the same profiles from Carlo glaciation-aged sites on the west side of the Nenana River valley from both LiDAR DTMs and IfSAR DTMs. Then calculated *k* for each data set using the same methods as described above. The difference between *k* values from LiDAR and IfSAR is the "*k* correction" value. This value was used to correct raw *k* values and present both the raw and corrected average *k* values in the results.

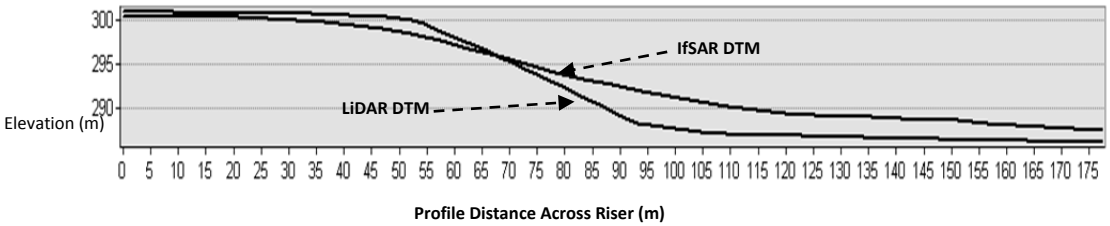


**Figure 1.9 LiDAR versus IfSAR Topographic profiles across the same riser.** This figure compares two slope profiles extracted from the same spot but one was extracted from an IfSAR DTM and one from a LiDAR DTM. The smoothing effect of the IfSAR is very apparent in this example and visually demonstrates why there may be a difference between the two when it comes to calculating k values.

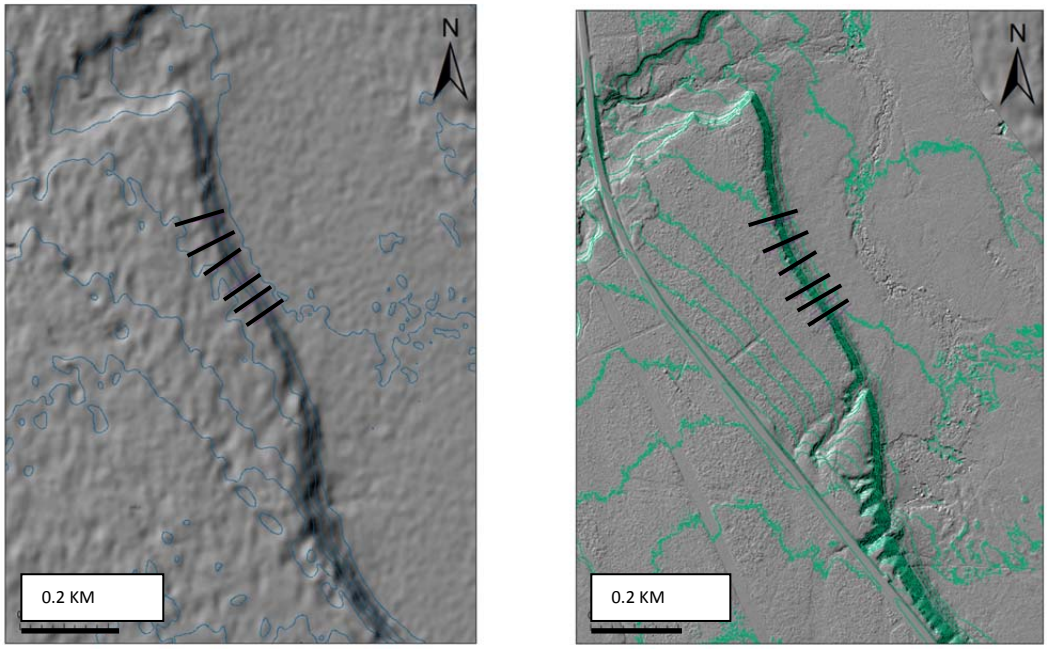


**Figure 1.10 a, b, c: Comparison of aerial photo (a), IfSAR (b), and LiDAR (c).** These three images were taken of the exact same spot on a Carlo-aged terrace riser on the west side of the Nenana River valley. The smoothing imparted by the lower resolution IfSAR is apparent here as it lacks to sharp edges of the LiDAR.

## 1.4. Results

### *1.4.1 Overview*

This study has three key goals; determining hillslope diffusion rates in the boreal forest, how these rates change with time and climate, and examining the effect of aspect on hillslope diffusion in this region. The most critical factor for accurate results is finding terrace risers that exhibit evidence of only been acted on by diffusive processes. Terraces that fit these criteria are characterized by minimal post-abandonment modification with negligible gullying, slumping, and other obvious out of plane sediment transport (such as active downcutting). Second, I collected topographic profiles from the selected risers and calculated their midpoints and maximum gradients. Then, coupled with other variables (age, critical hillsope gradient, maximum gradient and area of sediment moved on each individual riser), I calculated *k* values along risers encompassing four different aged surfaces and different aspects. Third, I compared diffusivity values across time and aspect. Finally, for three separate risers I compared data from the exact same profile but taken from IfSAR versus LiDAR with the expectation that higher resolution data would result in lower diffusivity. Once the discrepancy between the two data sources was calculated I created a "*k* correction factor" using the difference between the two and corrected my average *k* values accordingly for all of my sites.

*1.4.2 Results of k Calculations*

The results of IfSAR *k* calculations for the Nenana River valley regions show an average diffusion rate of 0.0025 ± 0.000767 $m^2$/yr (Table 1.2). These results include data from slope transects across terrace risers of three different landform ages in the Nenana River valley (Figure 1.4-1.6) for a total of 36 individual profiles; 12 per age group with these 12 each split up into generally north-versus south-facing slopes. Age errors on *k* values are included and range from 11 x $10^{-5}$ $m^2$/yr – 1.7 x $10^{-3}$ $m^2$/yr. Based on an ANOVA: Single Factor test producing an SSB of 0.000114 and a P-value of 0.09, there is a strong positive relationship and no statistically significant difference in diffusivity between the three landform ages. After calculating the diffusion rates I plotted my average k values as a function of landform age for each of the three age groups (Figure 1.11), to determine the relationship between diffusivity rates, age, and glacial cycles.

TABLE 1.2. k VALUES FOR THE NENANA RIVER VALLEY, ALASKA

| Sample ID | K ($m^2$/t) | Number of Samples |
|---|---|---|
| Healy (west side north-facing) | 0.0021± 0.0001 | 6 |
| Healy (east side north-facing) | 0.0025± 0.0002 | 6 |
| Healy (average) | 0.0024± 0.000011 | 12 |
| Riley Creek (north) | 0.0071 ± 0.0001 | 6 |
| Riley Creek (south) | 0.0021± 0.0004 | 6 |
| Riley Creek (average) | 0.0046 ± 0.000748 | 12 |
| Carlo (north) | 0.0032± 0.0017 | 6 |
| Carlo (south) | 0.0034± 0.0015 | 6 |
| Carlo (average) | 0.0033± 0.00147 | 12 |
| All NE and N facing average | 0.0037± 0.000572 | 18 |
| All SW and S facing average | 0.0027± 0.000962 | 18 |
| Overall Average | 0.0025± 0.000767 | 36 |

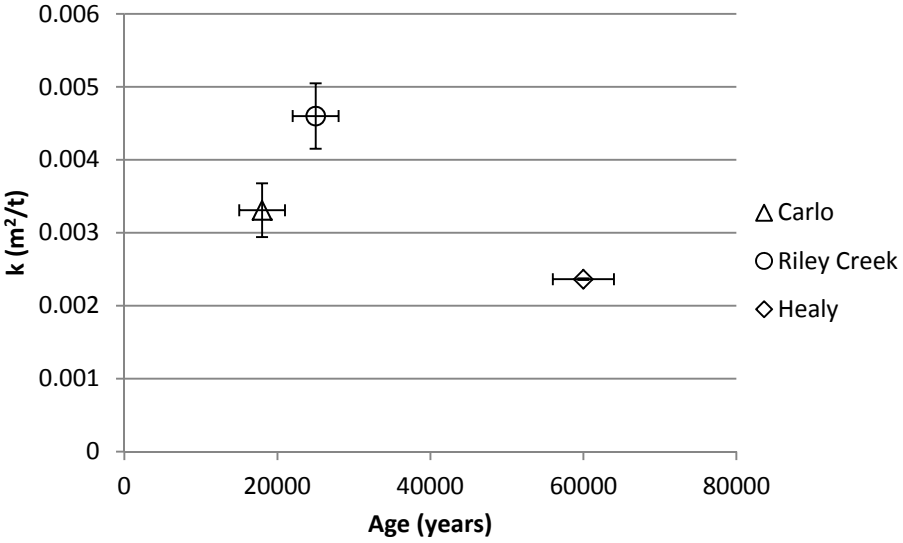


**Figure 1.11 Diffusivity versus landform age (uncorrected values):** This plot shows average k values for each individual landform age with error on both *k* and age (from youngest to oldest Carlo, Riley Creek, and Healy) versus diffusivity values. Where error in *k* is too small to be clearly displayed on this scale it equals 0.00001 $m^2$/year (Healy glaciation).

*1.4.4 k Correction Factor*

The results of the IfSAR versus LiDAR calculations show a consistent difference between the two data sets, with LiDAR DTM *k* values averaging 0.0017 $m^2$/year, which is 0.001 $m^2$/year less than the average IfSAR DTM value of 0.0027 $m^2$/year on the same landforms. Using this average difference I propose a "*k* correction" for values obtained from IfSAR data to account for the error introduced by the lower accuracy of this data set when compared to LiDAR. This *k* correction is equal to the difference between the calculated average LiDAR *k* values versus the IfSAR *k* values (0.001 $m^2$/year) (Figure 1.12, Table 1.3). This assessment shows that use of IfSAR data does overestimate *k* and is critical factor that must be included to produce representative *k* values, but that the overestimation in some cases may be corrected using data from the limited higher

resolution LiDAR data from this region. I applied the correction value to each of my average *k* values for all sites including Carlo, Riley Creek, and Healy on both sides of the Nenana River (Figure 1.13, Table 1.4). Although the overall average *k* value for IfSAR was larger, there is a strong positive relationship between the two and no statistically significant difference, based on a paired t-test producing a Pearson's Correlation of 0.64 and a P-value of 0.5.

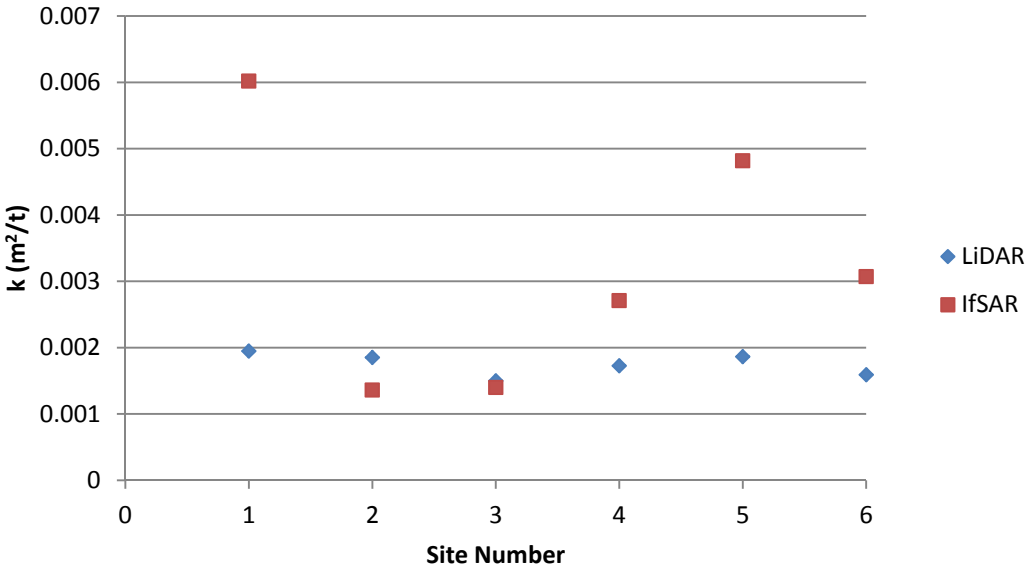


**Figure 1.12: IfSAR versus LiDAR *k* values for Carlo landforms.** This figure shows a comparison of calculated *k* values for the same landforms but with IfSAR data (red) and LiDAR data (blue). The X-axis corresponds to the six Carlo-aged riser profiles on the west side of the Nenana River (CAW) where, 1= CAW1, 2= CAW3, and so on. The difference between the two averages 0.001 $m^2$/year larger for the data extracted from IfSAR due to the lower resolution and subsequent smoothing imparted by this dataset.

TABLE 1.3. CORRECTED K VALUES FOR CAW PROFILES

| Sample ID | IfSAR k ($m^2$/t) | LiDAR k ($m^2$/t) | Corrected k($m^2$/t) |
|---|---|---|---|
| CAW1 | 0.006 ± 0.0013 | 0.0019 ± 0.000433 | 0.005 ± 0.0013 |
| CAW2 | 0.0014± 0.00099 | 0.0019 ± 0.000412 | 0.00039± 0.000999 |
| CAW3 | 0.0014 ± 0.00557 | 0.0015± 0.000333 | 0.00042± 0.00557 |
| CAW4 | 0.0027 ± 0.0001 | 0.0017 ± 0.000383 | 0.0017± 0.000383 |
| CAW5 | 0.0048 ± 0.0002 | 0.0019 ± 0.000414 | 0.0039± 0.000414 |
| CAW6 | 0.0027± 0.000011 | 0.0016 ± 0.000353 | 0.0018 ± 0.000353 |

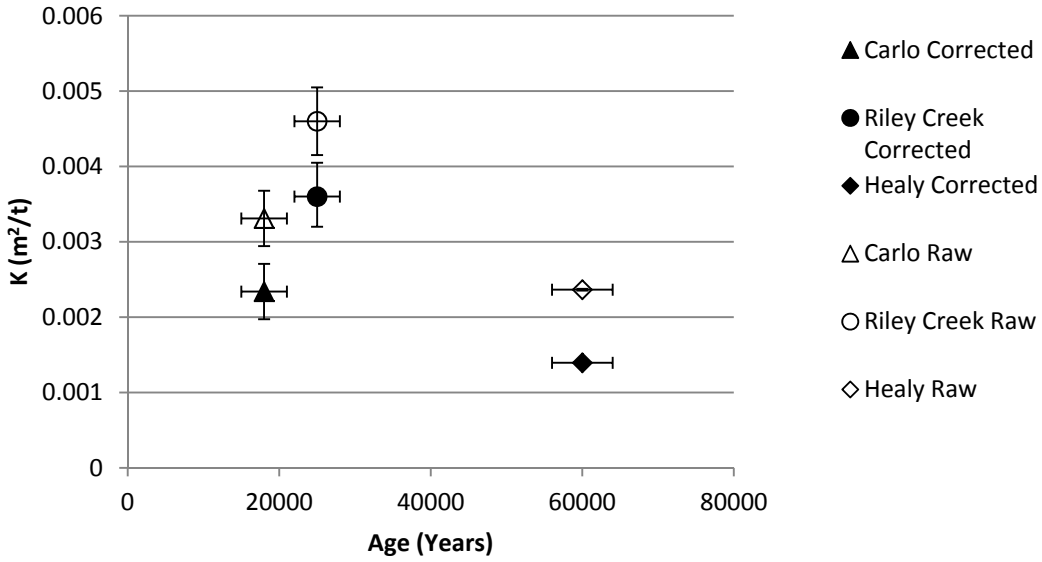


**Figure 1.13 Diffusivity versus landform age raw and corrected average values.** Open symbols show raw values and filled symbols show corrected values using the "*k* correction factor" of 0.001 $m^2$/year. Error for the Healy average is too small to show on this scale and equals 0.00001 $m^2$/year.

TABLE 1.4. CORRECTED k VALUES

| Sample ID | Raw k | Corrected k | Sample Number |
|---|---|---|---|
| Healy (west side north-facing) | 0.0021± 0.0001 | 0.0011 ± 0.000073 | 6 |
| Healy (east side north-facing) | 0.0025± 0.0002 | 0.0015 ± 0.0001 | 6 |
| Healy (average) | 0.0024± 0.000011 | 0.0014 ± 0.000093 | 12 |
| Riley Creek (north) | 0.0071 ± 0.0001 | 0.0061 ± 0.0085 | 6 |
| Riley Creek (south) | 0.0021± 0.0004 | 0.0011 ± 0.00013 | 6 |
| Riley Creek (average) | 0.0046 ± 0.000748 | 0.0036 ± 0.000432 | 12 |
| Carlo (north) | 0.0032± 0.0017 | 0.0022 ± 0.00037 | 6 |
| Carlo (south) | 0.0034± 0.0015 | 0.0034 ± 0.0015 | 6 |
| Carlo (average) | 0.0033± 0.00147 | 0.0033 ± 0.00147 | 12 |
| All NE and N facing average | 0.0037± 0.000572 | 0.0027 ± 0.000572 | 18 |
| All SW and S facing average | 0.0027± 0.000962 | 0.0017 ± 0 | 18 |
| Overall Average | 0.0025± 0.000767 | 0.0015 ± 0.000767 | 36 |

*1.4.3 Aspect versus k*

This study was limited to a narrow range of aspects because the only suitable risers were roughly parallel to the NNW-trending Nenana River. East-west trending tributaries are present in the valley, but they do not contain risers of a known or inferred age. To examine the effect of aspect on *k* values, I determined the azimuth direction of each individual riser face by making shapefiles in a GIS (ESRI) of six profile lines for each landform on each side of the Nenana River (the lines ranged from ~100-300 meters long across the riser), determined the directional mean of each line within the shapefile, and plotted each direction as a function of the corresponding *k* value for each riser profile. When *k* is plotted as a function of azimuth (Figure 1.14) no significant relationship is seen. The variation in azimuth for risers on the east side of the river was ~ 11 degrees, and for those on the west side was ~28 degrees and does not vary enough to expect substantial difference in diffusivity rates. The results of a paired t-test show no significant difference between my two data sets. Since the suitable terrace risers available for this study encompass a limited variation in aspects, this analysis of the influence of slope aspect on diffusivity is inconclusive. I tested the statistic significance of my values using a paired t-test. Since this test produced a Pearson's Correlation of 0.4, indicating a strong positive relationship between the two data sets and a p-value of 0.18, i.e. greater than 0.05 (5 %), showing no significant difference between the two, it can be concluded that there is no statistically significant difference between my two data sets.

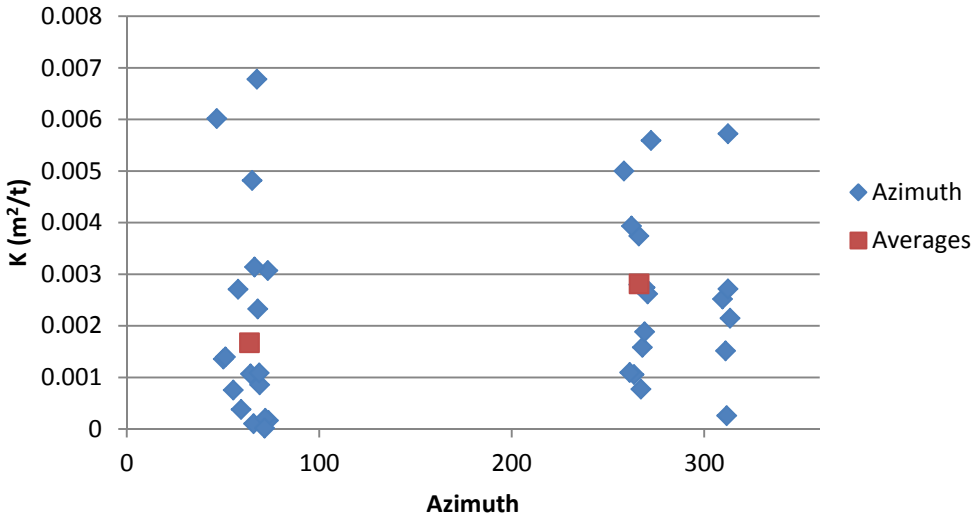


**Figure 1.14: Diffusivity versus riser azimuth.** This plot shows *k* values for both sides of the Nenana River valley plotted as a function of their individual azimuth. Average for each side of the valley were 64° (west side) and 266° (east side). No significant difference in *k* value is seen between the two general aspects in question.

### 1.5. Discussion

I addressed the first question of what are hillslope diffusion rates in the boreal forest environment by utilizing elevation and profile length data to solve a nonlinear hillslope diffusion equation. Overall, the results of my *k* calculations do not support the original hypothesis that hillslopes in the boreal forest degrade slower than those in mid-latitude environments, but instead, the corrected *k* values fall within the lower range of those previously reported for other regions.

Comparing the resulting diffusivities as derived from two different, moderate to high-resolution DEMs are mainly included as a quality control test of my IfSAR data. The majority of risers in my study area are not covered by LiDAR so it was necessary to use

IfSAR DEMs, which we predict to produce artificially high diffusivity rates. Use of the IfSAR data does result in mostly larger *k* values than use of the LiDAR data. Based on these results I implemented "*k* correction" factor to apply when using IfSAR data instead of LiDAR, which will effectively "correct" for the lower-resolution of the IfSAR data. It is important to note that this *k* correction factor is only appropriate for this particular study site but the same technique could be implemented in other locations. The difference between the average *k* values with IfSAR data versus LiDAR is 0.001 $m^2$/year with the average LiDAR values equal to 0.0017 $m^2$/year and average IfSAR values equal to 0.0027 $m^2$/year for a set of profiles on Carlo-aged surfaces. Although two IfSAR points are smaller than the LiDAR points the key is that the IfSAR points are not consistent with each other due to smoothing and low resolution, and the LiDAR data points are consistent. Even though I have only documented this discrepancy for one landform the correction factor has been applied to the *k* values for the Nenana River Valley. These values should be representative based both on the generally smaller *k* values obtained from LiDAR data, as well as the visible smoothing seen in the IfSAR profile (Figure 1.9), which mimics a faster rate of degradation.

Hanks (2000) summarized reported *k* values for several locations for a variety of landforms which range from 0.016 $m^2$/year for the Raymond Hill fault in Pasadena, CA to 0.0001 $m^2$/year in southern Nevada and are included in Table 5. Although this table includes values for fault scarps, stream terraces, lake shorelines, and fluvial terrace risers, the most appropriate comparison to *k* values of the Nenana River valley would be the fluvial terrace risers based on the similarities in formation history and initial riser

geometry. Fluvial terrace risers in any environment will undergo a similar process of formation, deposition, and abandonment through time; therefore it should be reasonable to compare their values across time and space (i.e. different regions, climates and ages). Interestingly, the fluvial terrace riser *k* values presented in Hanks (2000) table are larger than values in the Nenana River valley, particularly when I apply the correction factor of 0.001 $m^2$/year to the original raw value of 0.0025 $m^2$/year, resulting in 0.0015 $m^2$/year. This result highlights the complex interplay between of all the factors contributing to diffusivity.

TABLE 5. WORLD WIDE k VALUES

| Site | k ($m^2$/t) | Source[a] |
|---|---|---|
| Bonneville/Lake Lahontan, UT | 0.00064 | Hanks and Andrews (1989) |
| Fluvial terrace risers, SW MT | 0.002 | Nash (1984) |
| Lost River fault, antecedent scarps, ID | 0.0004 | Hanks (2000), |
| Machette Constraint on "unobservable" scarps, S. NV | 0.0001 | Hanks et. al (1984) |
| Bare Mountain fault scarps, S. NV | ~0.0001 | L.W. Anderson (personal communication with Hanks, 2000) |
| Lake Lisan recessional terraces, Dead Sea Area (Israel) | 0.0004 | Bowman and Gerson (1986) |
| Fault scarps, Northern Arava (Israel) | >0.0004 | Bowman and Gross (1984), |
| Stream terraces, northern Negev (higher level) (Israel) | >0.0001 | Begin (1992), |
| Stream terraces, northern Negev (lower level) (Israel) | >0.0002-.0007 | Begin (1992), |
| Fault scarps, southern Arava (Israel) | 0.0002-0.0003 | Enzel et al. (1995) |
| Fault scarps, Gansu Province (Western China) | 0.003 | Tapponnier et al. (1990) |
| Fluvial terrace risers, Dzungarian Basin (Western China) | 0.0055 | Avouac et al. (1993) |
| Fluvial terrace risers, Tarim Basin (Western China) | 0.0035 | Avouac and Peltzer (1993) |

| | | |
|---|---|---|
| Uplifted marine terraces, Santa Cruz | 0.011 | Hanks et al. (1984) |
| Raymond Hill fault, Pasadena | 0.016 | Hanks et al. (1984) |
| San Andreas fault, Carrizo Plain | 0.0085 | Arrowsmith (1995) |
| Lake Algonquin shoreline (MI) | 0.0012 | Nash (1980) |
| Lake Nipissing shoreline (MI) | 0.0012 | Nash (1980) |
| Oregon Coast Range | 0.0023 | Roering et al. (1999) |
| Nenana River valley, AK (raw) | 0.0025 | This Study |
| Nenana River valley, AK (corrected) | 0.0015 | This Study |

[a]Full references can be found in (Hanks, 2000)

The corrected average *k* value of 0.0015$m^2$/year is most similar to the diffusion rates of those from shorelines of Lake Algonquin and the Oregon Coast Range, both of which are included in Table 5. This is curious because each site represents a different biome; the Nenana River valley occupies a boreal forest environment, Lake Algonquin is located in a hemi-boreal climate, and the Oregon Coast Range is a temperate rainforest.

In terms of the values reported for *k* world-wide, there is a general convergence of *k* values around ~0.001$m^2$/year for late Quaternary alluvial materials in the Basin and Range area of the western U.S (one of the most intensely studied areas in the context of scarp and hillslope diffusion). According to Hanks (2000), the world-wide reported variability of *k* from 0.0002 $m^2$/year (Israel) to up to 10 times larger in parts of California (0.0085 $m^2$/year) are clearly climate-related (Hanks, 2000). The values I report for the Nenana River valley (average of 0.0015 ± 0.00074 $m^2$/year), fall roughly in the low to middle portion of the spectrum. Hanks (2000) also notes that constraints of *k* for pre-Holocene landforms are scarce and uncertain, mainly due to the climatic influences related to glacial and interglacial cycles and the added complications associated with

these drastic climatic shifts. Since the landforms of the Nenana River valley correspond to regional glaciations there are possible variations in diffusivity related effects of glacial cycles on diffusive processes. However, the results of this study did not show significant differences between terrace risers corresponding to different glacial cycles. My reported *k* values are accurate for this region, regardless of the glacial influence, this study is concerned with the time since the abandonment of these terrace risers when diffusive processes became the dominant force acting upon them.

Further analysis and interpretation of *k* values facilitates the comparison of *k* versus landform age to address how the values might change over time and with climate. Comparing average *k* values versus their landform age (Figure 1.13) to look for a trend between age, climate, and diffusion rates. The landforms are all within a similar range, which suggests that over time *k* may fluctuate with climate, specifically in relation to glacial versus interglacial cycles but it seems to remain relatively consistent. Between the three glaciations Riley Creek is the smallest *k* value, Carlo exhibits the largest *k* value, and Healy is in between the two. Although the three average diffusion rates are not within the error of one another they are not largely different either. Therefore, Sampling from landforms formed during interglacial cycles, may enable one to see an alternating pattern of low and high degradation during glacial versus interglacial cycles, but with the current data this argument cannot be made.

To address the third question of the effect of aspect on diffusion rates, I compared *k* values to their respective azimuth  This question is formulated, in part, after Clarke and Burbank (2010) who observed that not only did riser gradient decrease as a

function of decreasing riser height but, equator-facing risers degraded twice as fast as those facing the poles. Clarke and Burbank (2010) attribute this behavior to be a function of the amount of solar radiation received by each respective riser, which in turn controls maximum vegetation biomass, regolith and soil development rates. Calculated *k* values do suggest the same behavior in the boreal forest with generally south-facing risers degrading faster than those generally facing north although the difference is not significant when *k* is plotted as a function of azimuth. The results related to the third question demonstrate that contrary to the original hypothesis, even if controls on hillslope diffusion might be unique in the boreal forest, hillslope diffusion itself still abides by the same behavioral regime as has been observed in other regions.

### 1.6 Conclusions and Future Work

Hillslope diffusion rates have been reported for several regions and can be grouped by climate and biome based on where they fit in the global spectrum. The hillslope diffusion rates produced in this study for a boreal forest environment fit in the lower end of the spectrum near to hillslope diffusion rates for a hemiboreal region. This new data helps to both fill a gap in world-wide hillslope diffusion rates and gives us a reference point for current rates in the boreal forest with regards to potential changes related to climate change. This study addressed three main questions related, more specifically, to hillslope diffusion processes. First, I calculated average *k* values as well as a "*k* correction factor" (equal to 0.001 $m^2$/year), which was applied to raw *k* values; second, I analyzed and compared results to answer the question of how *k* varies with

climate and time; and third, I plotted *k* as a function of azimuth to address the question of how aspect affects hillslope diffusion in the boreal forest.

Results show diffusion rates within the range of values reported for Lake Algonquin, MI., shorelines as well as forested hillslopes of the Oregon Coast Range. I also saw a slight difference in rates between glacial cycles. To address the question of the effects of aspect on hillslope diffusion I averaged generally north-facing and generally south-facing risers and calculated the error both in age and *k* values for both. There was not a clear trend between aspect and *k* value or significant difference between the two populations so I concluded that aspect does not play a significant role in diffusion rates (at least on NNW trending risers such as those in the Nenana River valley). I confirmed that hillslope diffusion processes follow the same principles and predictions seen in other environments, even if the controls are different, for example, the insulating effect of snow cover, or the role of trees in downslope sediment transport, by reporting *k* values similar to those in both Michigan and Oregon. It is my hope that the results of this study will serve as a baseline for future studies in this region and field of expertise.

Future work to build on this study would include collecting a more robust data set to test these trends between diffusion rates and aspect over a larger region, or perhaps calculate k values for several discrete regions. In addition, a larger test of LiDAR versus IfSAR across time and space would be useful for a more complete quality control check. A larger study region could provide a general trend of k values over this region, but comparing several separate areas could provide insight into the variability of k and

how it might vary geographically. Another point of interest for future work would be constraining the specific controls on *k* and their relative contribution to the diffusion process. This would likely be a long-term observational study involving some type of sediment movement monitoring stations, detailed soil surveys, permafrost monitoring, potentially utilizing ground penetrating radar (GPR), root density calculations (this could be done using GPR as well), and more rigorous age constraints on all landforms involved.

## Chapter Two:

## Effects of depositional history and provenance on quartz luminescence dating: a case study in the Nenana River Valley, central Alaska

### 2.1. Introduction

Determining the geologic sources and previous depositional or pedogenic history of a given sampling site is an essential step in any Quaternary dating method (Duller, 2008; Rhodes, 2011). With regard to optically stimulated luminescence (OSL ) dating, factors such as depositional and formation history of the deposit to be dated can affect everything from sampling procedure to the interpretation of results. A deficient depositional history ( i.e. meager or no repetition of erosional and depositional cycles), can mean that the quartz exhibits decreased sensitivity in the natural luminescence signal (Duller, 2008).

In addition, young source rocks, particularly those of a volcanic, hydrothermal, or a particular kind of sedimentary origin (i.e., limestone), can contain quartz and feldspar that emit thermally unstable, medium or slow OSL components and high recuperation signals (Fathai, 2003; Steffen et al., 2009; Tsukamoto et al., 2007) instead of the required fast OSL component needed for the commonly utilized single aliquot regenerative (SAR) procedure. Wintle and Murray (2006) suggest that it is only prudent to work in the range where the natural signal (LN /TN) is 85% or less of the maximum measured luminescence signal, but this is difficult to control or predict (Duller, 2008). Resetting of the sediments from glacial bedrock or ice-bed interfaces (stress induced

bleaching and friction-induced dosing) are adequately covered in Bateman et al. (2012) and will not be discussed further here.

Understanding the nature of the recent geologic past in the Nenana River valley is not only important for increasing our knowledge of how ice-free regions form and react to changes in climate, but this information helps to advance current ideas which couple continuous global records with independent and robust age control. Although Alaska's loess record has been dated using radiocarbon and OSL (Begét et al., 1990; Berger, 2003; Muhs et al., 2003; Pewe, 1955; Péwé, 1975a; Roberts, 2012), relatively few researchers have attempted to date the frontal glacial deposits and associated fluvial terraces (Dortch, 2006; Dortch et al., 2010; Reuther, 2013), or understand the influence that the source geology has on meaningful OSL data. The success of OSL dating in Alaska is partly dependent on the regional geology, which affects the sensitivity and other luminescence characteristics; variations in the type, composition, cooling rates, thermal history and properties of dated minerals, as well as differences in the depositional environments in which the minerals are found (Sawakuchi et al., 2011).

If a basic protocol can be developed prior to ever going into the field, this knowledge can prevent surprises or disappointments after the fact. Our approach is to synthesize our experience with quartz OSL applications in the Nenana River valley of central Alaska (Figure 2.1) as a case study to address this problem and to give insight into ways in which scientists can become more informed as to how the geology of their site and associated luminescence characteristics may inform them of the best deposits to sample.

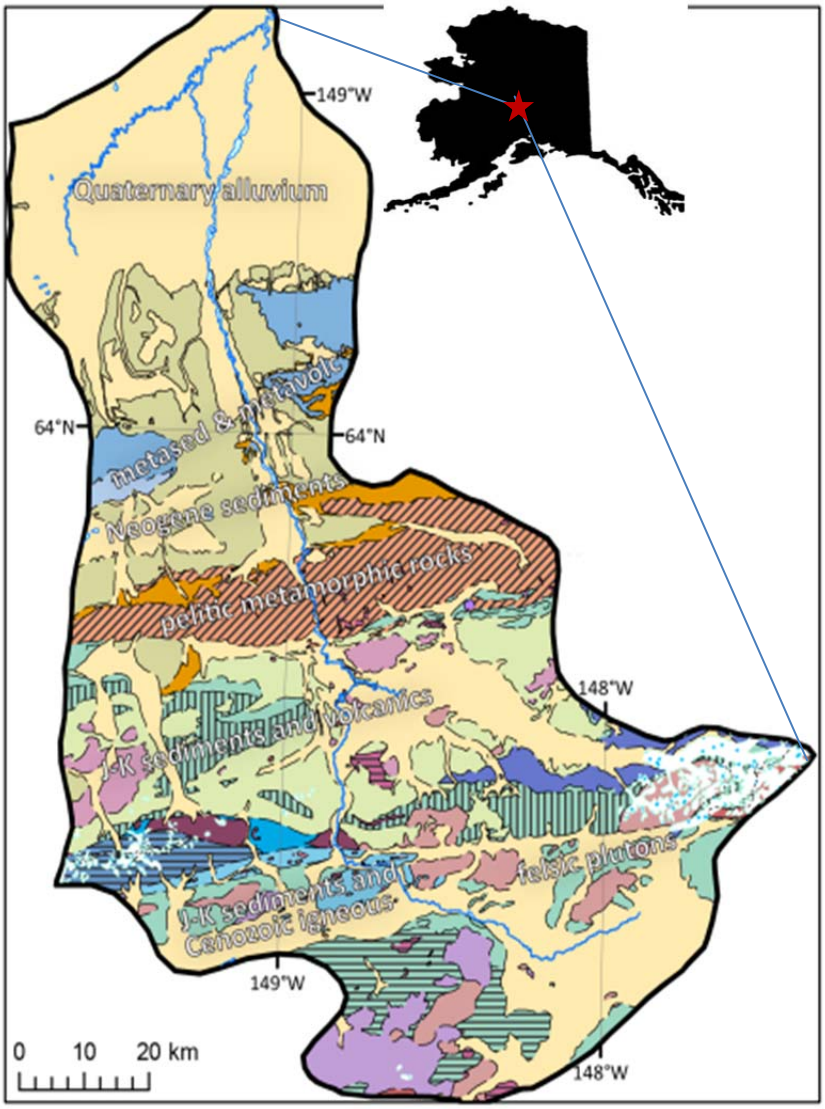


**Figure 2.1: Study location and geology of Nenana River valley**. The locus of the case study is shown by the red star situated just north of the Alaska Range in central Alaska. It can be seen from this figure that the source rocks for sediments found in this area include plutonic, volcanic, and metamorphic terrains, which contributes to the complex unraveling of the geologic history of samples.

It is, therefore, a necessary and important step to determine the appropriate luminescence method for Alaska geology by synthesizing previous research using OSL or other Quaternary geochronological techniques, such as *in-situ* cosmogenic nuclide dating and then offering a decision-tree process whereby the field geologist can ascertain where best to sample. When we have a better knowledge of under what geologic circumstances the OSL method works for material in the Nenana River valley it can be applied to sediments in other regions. This will provide useful information for reconstructing sedimentological history and insight into climatic cycles. Many researchers have offered protocols and experiments designed to aid the researcher in getting the most reliable equivalent dose signal from quartz or feldspar (Roberts, 2012; Wintle, 2010).

## 2.2 Sampling and Methods

### *2.2.1 Field and Lab Procedures*

Seven OSL samples were taken from fine-grained fluvial sediments and terrace capping loess (Figure 2.2). We selected sites based upon the availability of existing natural exposures and the ability to establish that the exposed sediments were not reworked. We were able to determine that the lack of reworking in the sediments based on the absence of mixing due to frost and bioturbation. At each site, several centimeters of the surface was scraped away in order to remove any slumped and/or bleached sediment before sampling. Samples were collected by filling PVC tubes (eight inches long by one and a half inches in diameter) and taken perpendicular to the vertical exposures. The ends of tubes were sealed with PVC caps and black electrical tape, and

the sealed tubes were rolled in heavy-duty black garbage bags. OSL samples were processed at the United States Geological Survey (USGS) Luminescence lab in Denver, CO.

**Figure 2.2: Sample Sites.** PC-OSL3b (left, see Table 2) where an OSL sample was taken in a sandy glacial deposit. The picture at right is from the SL-series (Slate Creek Site where OSL samples were taken from the loess as well as sandy fluvial deposits). This particular picture is SL1-OSL2 (see Table 2.2). Scale is denoted by the Japanese razor hoe (30 cm in length) in the left-hand photo and the pink surveyor's flagging (1.25 cm wide) in the right-hand photo.

*2.2.2 OSL equivalent dose methods*

At least 5 cm of sediment was removed from both ends of the OSL sampling tube under "safe light" (i.e. sodium vapor lighting) conditions in the luminescence laboratory. The ends and the middle portion of the samples were dried in an oven at 40 $^{o}$C. The middle part of the sample was sieved to collect both fine (< 90 μm) and coarse grained fractions (with fractions between 90-250 μm). The entire sample was leached in 5N HCl (15% HCl) for 24 hours, 30% $H_2O_2$ for 24 hours, and then sieved. The coarser grained size (90-250 μm) quartz fractions were separated from the feldspars and any heavy minerals using a Franz magnetic separator and heavy liquids (lithium sodium polytungstate or LST) ($\rho$ = 2.58 gcm$^{-3}$). To remove feldspars and to isolate pure quartz from the selected sand fraction, we centrifuged the sand sequentially in the LST. The densest grains that separated from the 2.58 gcm$^{-3}$ were subjected to a 50% solution of HF acid for 50 minutes while in an ultrasonic bath. After pouring off the HF solution, we put the sample in 8N HCl for five minutes (still in the ultrasonic bath) and finally re-sieved to winnow out broken feldspar grains. Steel target discs were sprayed with silica spray and a single grain thick layer of quartz grains was dispersed onto the steel discs. Feldspar grain separates were lightly etched in 50% HF for 10 minutes, washed in distilled water, and stored.

Continuous Wave Blue LED stimulated-OSL was measured on fine sand-size quartz separates using single aliquot regeneration (SAR) protocols (see Table 2.1). Light stimulation of the quartz was achieved using a RISØ TL-DA-15 reader with an array of blue LEDs centered at 470 nm (15 MW/cm$^2$). Detection optics consisted of Hoya 2×U340

and Schott BG-39 filters coupled to an EMI 9635 QA Photomultiplier tube. β radiation was applied using a 25 mCi $^{90}Sr/^{90}Y$ built-in source. The main SAR parameters included use of the 40 second blue-diode wash step of Murray and Wintle (2003) at the same temperature as the preheat temperature. They included preferred component of SAR dating if it was dominant (i.e. the "fast" component of Murray and Wintle, 2000; Wintle and Murray, 2006; Rhodes 2011), a signal usually released in the first 0.8 seconds of a typical blue diode stimulation.

**TABLE 2.1: Luminescence parameters used in preparation and analyses of samples for quartz OSL for single aliquots**

| Measurement parameters: | |
|---|---|
| Machine | Automated Risø TL/luminescence-DA-20 |
| Mineral; grain size: | quartz: 250-180 or 250-150 μm |
| Stimulation source: | blue LED diodes, emission centered on 470 nm |
| Power delivered to aliquot: | 18 mW/cm$^2$ (85% power) |
| Duration of stimulation: | 40 seconds of continuous wave |
| Photomultiplier: | Thorn-EMI 9235QA |
| Aliquot temperature: | 125 °C |
| Detection filters: | two Hoya U340 filters |
| Preheat: | 240 °C (samples <5 ka) for 10 secs |
| Delay before measurement: | 120 sec |
| Equivalent dose evaluation: | single aliquot regeneration (*Murray and Wintle, 2000, 2003*) |
| Background evaluation: | black body counts <30 ct/sec, BG counts <40 ct/sec |
| Alpha effectiveness: | n/a |
| Dose-rate evaluation: | high-resolution gamma spectrometry (Ge detector) |
| Dose rate range: | 3.23-2.13 Gy/ka (Grays per thousand years) |
| Water content: | 75% of full saturation (depending on material and site) |
| Cosmic-ray contribution: | 9-7% of total dose rate, dependent on sampling site |

The choice of preheating temperature for each sample was based on preliminary tests and the experiences of others with samples of a similar nature from Alaska. All sample aliquots were run at 240 °C for ten seconds and several quality-control criteria were employed to reject OSL signals and resultant SAR equivalent dose values when needed (i.e., if decay curve signals were observed to be elevated above the baseline we rejected any subsequent data).

The growth of luminescence with increasing dose was generally not well represented by a single saturating exponential + linear function or an exponential function. We researched the test for a fast ratio comparison (Durcan and Duller, 2011) but we were not confident of our ability to cross-section our OSL signals, so we chose instead to employ the simpler sensitivity test over repeated SAR cycles (Figures 2.3a, b, c, 2.4 a,b,c, 2.5 a, b, c, and 2.6 a, b, c).

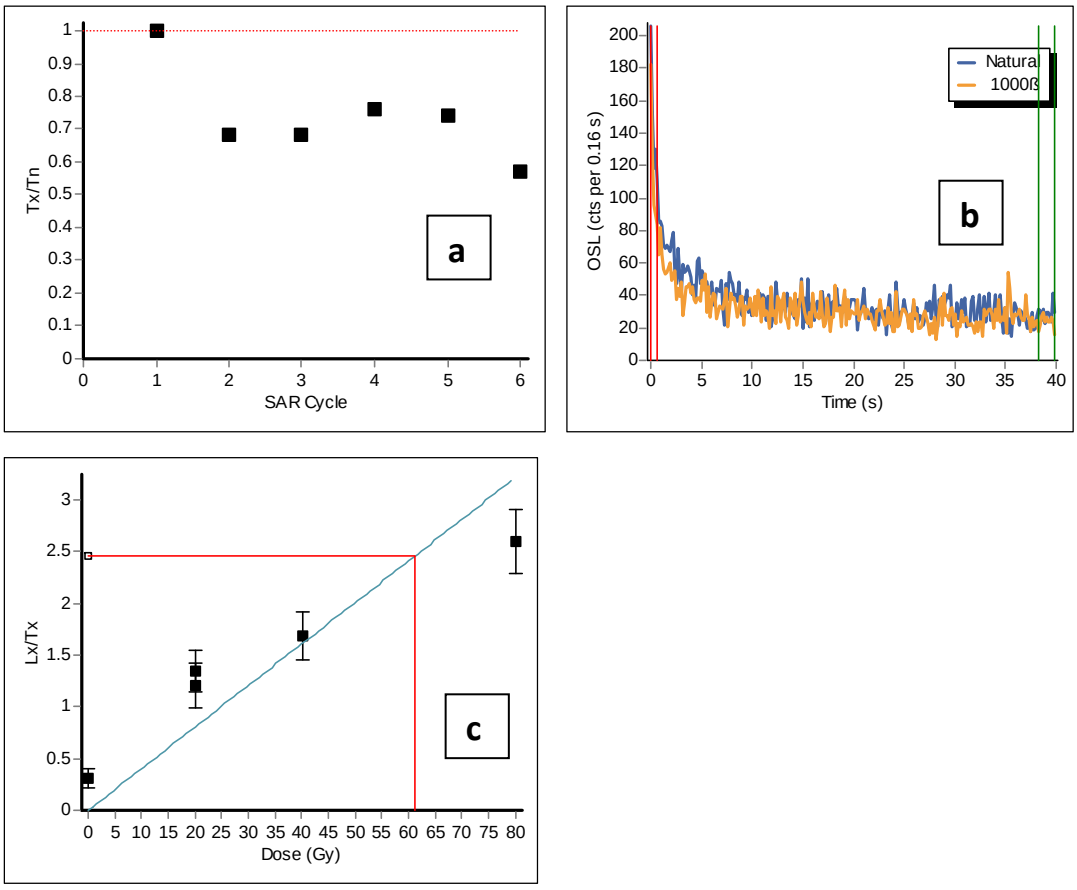


**Figure 2.3 a, b, and c.** This figure shows an example of sensitivity cycles, a decay curve, and a growth curve for **SF HFCF-T2-OSL1**. 2.3a shows the **falling ratio** obtained using the SAR protocol when the natural signal is plotted through successive SAR cycles. 2.3b shows the generally dim signal ("dim" because the curve is noisy and does not rise and then drop cleanly down to near zero for the remainder of the time) obtained even at the

start of the measurement (a bit over 200 photons/sec) and 2.3c illustrates the large errors for each measured radiation treatment in the growth curve.

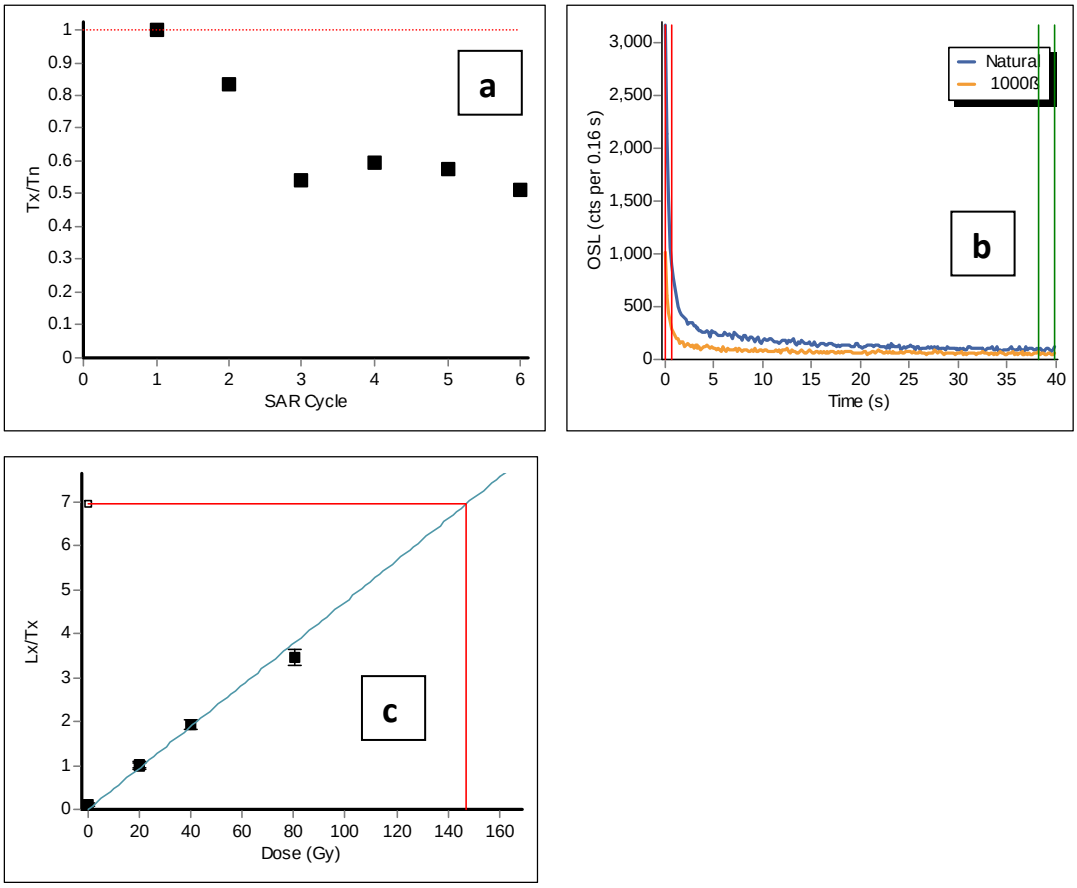


**Figure 2.4 a, b, and c.** This figure shows an example of sensitivity cycles, a decay curve, and a growth curve for **SF HFCF-T2-OSL1**. 2.4a again shows the **falling ratio** obtained using the SAR protocol when the natural signal is plotted through successive SAR cycles. 2.4b now shows a more robust signal ("robust" because the curve drops cleanly down to near zero after jumping up to ~3,000 photons/sec) obtained at the start of the measurement and 2.4c illustrates the smaller errors for each measured radiation treatment in the growth curve (although the natural is completely overwhelming the calibrated radiation doses).

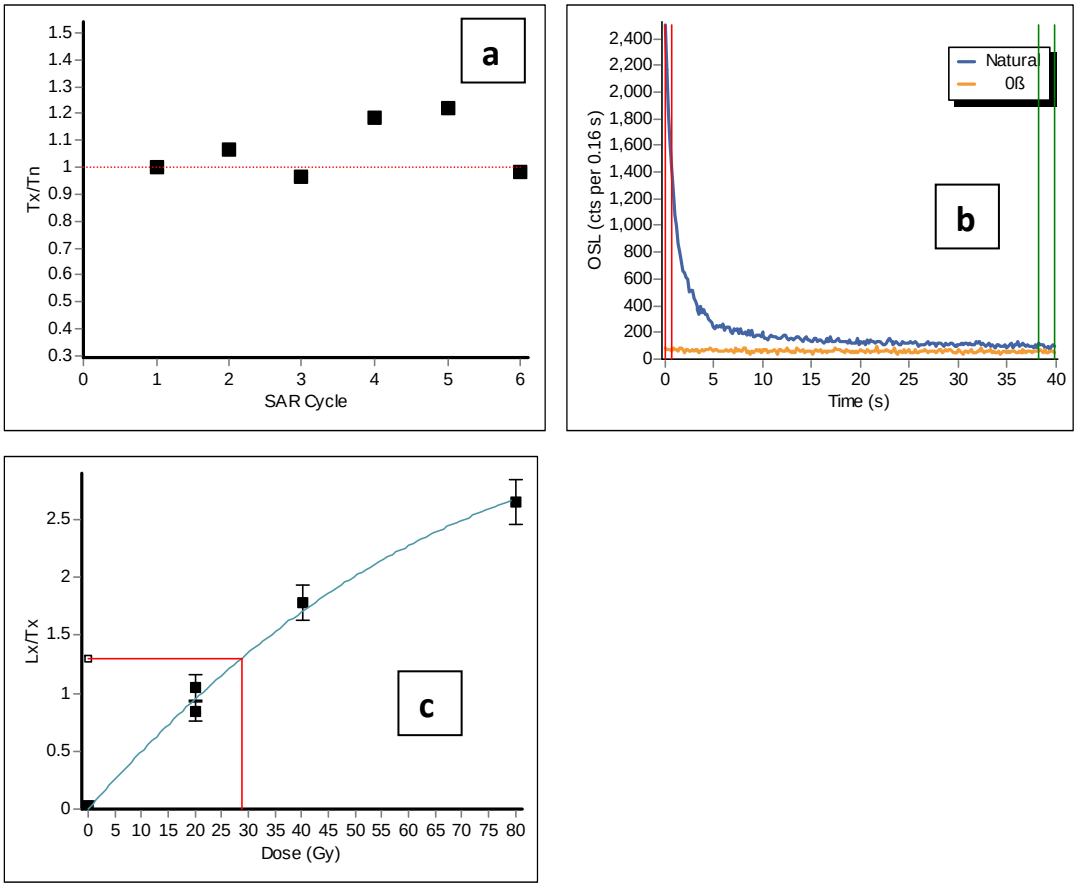


**Figure2.5 a, b, and c.** This figure shows an example of sensitivity cycles, a decay curve, and a growth curve for **PC-OSL3b.** 2.5a shows the even ratio of obtained using the SAR protocol when the natural signal is plotted through successive SAR cycles. 2.5b shows the **generally elevated baseline** of the signal obtained at the start of the measurement (a bit over 2,400 photons/sec) that is either an unstable fast component or feldspar contamination and 2.5c illustrates the large errors for each measured radiation treatment in the growth curve.

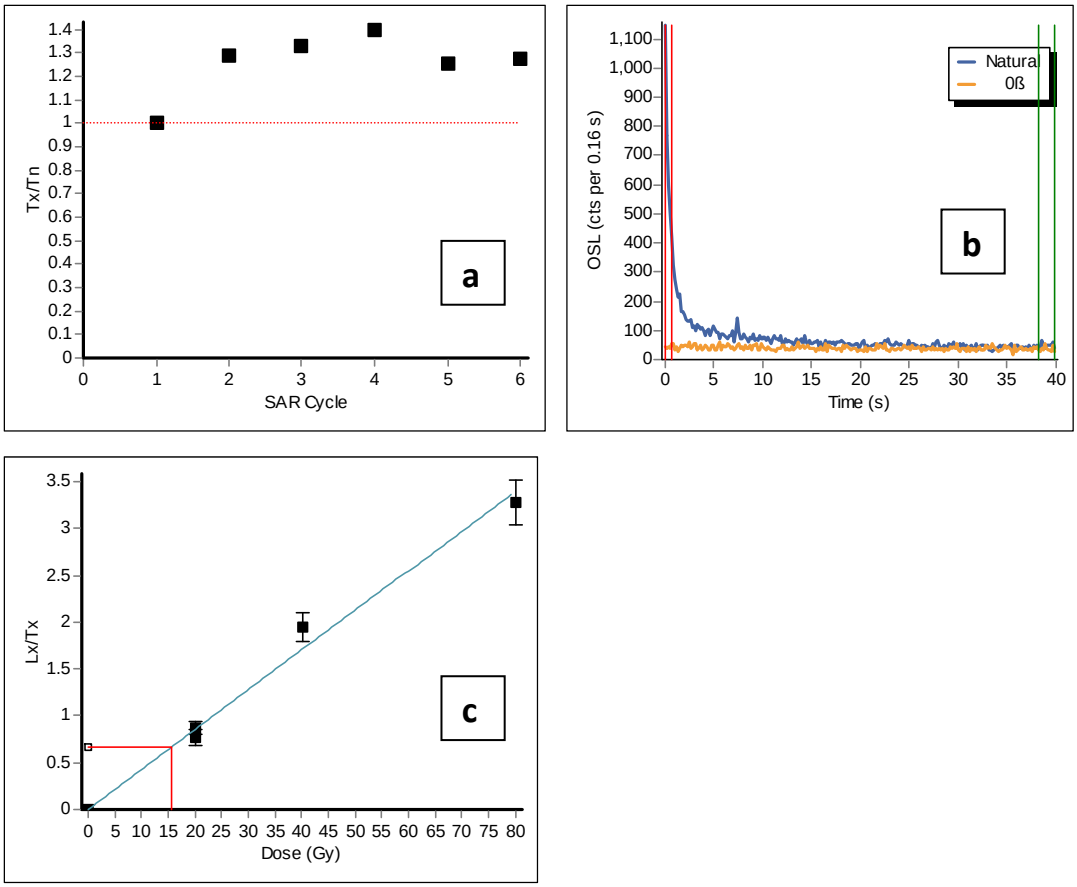


**Figure 2.6 a, b, and c.** This figure shows an example of sensitivity cycles, a decay curve, and a growth curve for **PT2-OSL1**. 2.6a shows the generally even ratio obtained using the SAR protocol when the natural signal is plotted through successive SAR cycles. 2.6b shows the generally **optimal large and fast component of the signal** obtained at the start of the measurement (a bit over 1,100 photons/sec) and 16c illustrates the small errors for each measured radiation treatment in the growth curve.

Data rejection criteria were similar to those in common practice (Wintle and Murray, 2006), and any acceptable growth curve data was fit to an exponential + linear trend. Most data did not pass our thresholds, which were: recycling ratios within 15% of

1.0, recuperation ratios within 2% of zero if recuperation was >20% of the normalized natural signal (Lx/Tx ratio), test-dose-signal errors of <10%, forcing dose-response curves through the origin, saturation behavior, a lack of proportionality between the regenerative and test-dose signals, and the above mentioned differences in sensitivity corrections between the natural and the regenerative cycles.

Obtaining reliable ages with OSL requires four main components, the natural luminescence signal measurement, an assessment of sensitivity (individual to each sample as discussed above), a measure of the luminescence signal response to applied radiation dose, and determination of the burial dose rate experienced by each sample (this will vary with geologic history of sample). When analyzing samples the first two steps are combined into one to produce the applied dose over the entire period of interest. This dose represents the amount of radiation energy deposited within the crystal since the last time it was exposed to daylight during transport, or heating, and is termed the equivalent dose or $D_E$, it is measured in the SI unit Grays (Gy; 1 Gy = 1 $J*kg^{-1}$) (Rhodes, 2011). The sample age is then calculated with the following equation (equation 5):

(5)

$$Age = \frac{D_E}{D_R}$$

Where, $D_E$ = equivalent dose and $D_R$ = dose rate (measured in Gy/Ka) and calculated mainly from the concentrations of radionuclides of K, U, Th, Rb in the sediments and lesser amounts of other cosmic ray components.

### 2.2.2 X-Ray Diffraction Methods

We selected three samples (Sl1-OSL3, SF-HCF-T2-OSL2, PC-OSL3) for analysis through x-ray diffraction methods at Vassar College. These samples were consisted of ~5 g selections from the processed OSL samples collected during summer 2012. Results of the X-ray patterns are included in Appendix B and annotated to explain what each peak represents. This analysis is just a preliminary test and will require a larger sample size in order to provide a more robust and updated mineralogical report of sediments in the Nenana River valley.

## 2.3. Regional Context

*2.3.1 Study Location and Climate*

Our study site is located in the Nenana River Valley on the north flank of the Alaska Range in the boreal forest biome (Figure 2.1). The Alaska Range acts as a barrier to precipitation coming up from the Gulf of Alaska (Muhs et al., 2001). Because of this, Pleistocene summers in central Alaska were relatively warmer and drier than other areas of Alaska, and kept the region ice-free during Quaternary glacial advances, with the exception of piedmont glaciers in north-flowing drainages along the northern side of the Alaska Range (Muhs et al., 2001; Péwé, 1975a). Based on these observations the absence of ice cover in parts of interior Alaska, as well as the northern flank of the Alaska Range, during the Quaternary glacial maxima is the key reason landforms and deposits from throughout this period are well-preserved in this area.

*2.3.2 Regional Geology*

In traversing the Alaska Range, the Nenana River derives sediment from three disparate geologic regimes (Figure 2.1). This river system begins on the south side of the Alaska Range, emanating from the Nenana Glacier and traverses westward along the south side of the Denali fault for 50 km when it abruptly turns north and crosses the Denali fault. In this section, the Nenana River crosses predominantly Jurassic-Cretaceous turbidite deposits (Kahiltna Assemblage), Paleogene felsic plutons, Triassic calcareous sediments, and a Cretaceous mélange (Csejtey, 1992). Further downstream, between the Denali and Hines Creek faults, the drainage system encompasses Devonian marine metasedimentary and metavolcanic rocks (the Yanert Fork sequence), Oligocene felsic plutons, a Cretaceous terrestrial to marine sedimentary sequence (Lower Cantwell Formation), Paleogene bimodal volcanics (Upper Cantwell Formation), as well as additional exposures of the Kahiltna Assemblage and Triassic calcareous sediments (Csejtey, 1992).

The Hines Creek fault is a major crustal geologic boundary (Brennan et al., 2011) with an abrupt transition in deformation and metamorphic history across the fault. To the north, and characterizing the rest of the Nenana River drainage system, is a crystalline basement dominated by regionally metamorphosed rocks with Precambrian and Paleozoic pelitic and volcanic protoliths (Dusel-Bacon et al., 2004; Wahrhaftig, 1968). This basement is characterized by predominantly phyllitic and schistose rocks, including quartz mica schist, mica schist, and quartzite in the lowermost unit and felsic and mafic metavolcanic and metavolcaniclastic rocks occurring as schists, phyllites, and

gneisses. The crystalline basement is overlain by a Neogene coal-bearing terrestrial sedimentary sequence (Usibelli Group) and a Plio-Pleistocene coarse grained alluvial sequence (Nenana Gravel; e.g.,(Csejtey, 1992; Péwé, 1966).

The Usibelli Group consists of fluvial and lacustrine deposits derived from predominantly south to southwest flowing streams, with sources from the crystalline metamorphic rocks of the Yukon-Tanana terrane to the north of the Alaska Range (e.g., Wahrhaftig 1987; Ridgway and Trop 1999; Ridgway et al. 2007). Coarse alluvial and braidplain deposits of the Nenana Gravel were deposited by north-flowing streams and this represents an abrupt drainage reversal corresponding with the development of the Alaska Range near its modern position (Wahrhaftig 1987). As a record of the unroofing of the modern Alaska Range, the Nenana Gravel is an archive of the diverse lithologies present in the upstream paleodrainage area (Ridgway et al., 2007; Thoms, 2000).

The late Cenozoic history of regional drainage reversals superimposed upon diverse rock assemblages due to the long history of terrane accretion and translation produces an inherently diverse suite of minerals within the recent fluvial and aeolian sediments of interior Alaska. The mineralogy of Quaternary Nenana River valley sediments is dominated by quartz, mica, plagioclase feldspar, and magnetite with microcline, biotite, garnet, and albite present in lesser amounts (Muhs et al., 2003). The presence of biotite-rich schist and phyllites in these sediments have been detected in X-ray diffraction (XRD) patterns for this study, supporting the mineralogy previously reported by Muhs et al (2003). As noted above, the majority of sediments of the Nenana River come from metamorphic, clastic, and plutonic sources, with lesser amounts of

clastic rocks of volcanic origin mixed in. This suggests that the lack of a fast component and unstable medium or slow components found in our quartz OSL samples is mainly due to a less than suitable depositional history and not the source rock itself.

### *2.3.3 Effects of Geologic and Geomorphic Processes on Sample Material*

#### *2.3.3.1 Availability of Datable Material*

Four types of deposits are generally available to the researcher for luminescence dating; aeolian, fluvial, lacustrine, and alluvial/colluvial sediment. This region is currently undergoing new research because of the recognition of a complex set of river terraces that are products of either deposition or erosion as the Nenana River adjusted to changing boundary conditions during glacial and non-glacial episodes of the growth of Nenana Glacier (Dortch, 2006; Dortch et al., 2010).

Aeolian deposits encompass any windblown material, including glacial and non-glacial silt as well as coarser-grained sand dunes. Loess is defined as wind-blown silt 20-30 micrometer in diameter (Ding et al., 1999). Loess is further categorized as derived from periglacial and non-glacial sources. Periglacial loess is derived from the floodplains of braided streams sourced from glaciated terrain. This glacially-derived loess is accumulated on floodplains during glacial periods and is transported and deposited during interglacial periods. Non-glacial loess deposits originate from dune fields, deserts, playa lakes and volcanic ash and include volcanic, tropical, and gypsum sources, as well the effects of transport mechanisms such as trade wind, and anticyclonic activity (Ding et al., 1999). One of the main differences between glacially and non-glacially derived loess is that glacially-derived loess is transported in a glaciofluvial system prior

to deposition and accumulation, which adds a component of partial bleaching not found in non-glacial loess sources.

*2.3.3.2 Variety of Datable Material*

*2.3.3.2.1 Regional Loess Cycle*

The most aereally extensive surficial deposit found in Alaska is loess (Muhs et al., 2003). Péwé (1955) determined that Alaskan loess was glacially derived, and since then the stratigraphy and depositional history of loess has been widely studied in central Alaska (Begét et al., 1990; Muhs et al., 2003; Pewe, 1955; Péwé, 1975a, 1975b; Westgate et al., 1990).

The pattern of loess production and accumulation varies regionally in Alaska through the Quaternary interglacial/glacial cycles. For example, the Gold Hill loess near Fairbanks shows thick paleosol development during Pleistocene interglacial periods, and thick sections of loess accumulated during glacial periods (Pewe, 1955). In contrast, Thorson and Bender (1985) argued that loess deposition in the Nenana River valley primarily occured during interglacial periods, and loess stripping occurs during glacial periods due to strong katabatic wind patterns. Muhs et al.(2003) also discuss findings from dust accumulation simulations which suggest that many parts of Alaska were important dust *sources* during the last glacial period, not during the Holocene. Effectively, glacial periods in the Nenana River valley present conditions favorable to loess *production*, and interglacial periods provide favorable conditions for loess accumulation.

*2.3.3.2.2 Fluvial Deposits*

Mapped fluvial and glaciofluvial deposits include fluvial terraces, outwash terraces, point bars, crevasse splays, fans, deltas, eskers, ox-bow lakes, channels, and levees. All of these deposits will differ in sedimentology based on sorting by the river. For example, a meandering river will produce finer-grained deposits while braided streams will produce heterogeneous deposits of generally coarser size. Since terraces are often preserved in various parts of the valley, this study mainly focuses on them. The suitability of fluvial terraces for OSL dating depends largely on the depositional nature of the river (Sawakuchi et al., 2011), but can also depend on source material (Preusser et al., 2006; Zheng et al., 2009). Glaciofluvial rivers are turbulent and narrow channeled in the mountains, resulting in partial bleaching of sediments as well as resultant poor luminescence characteristics. Outwash terraces in particular, are not only a part of this turbid, glaciofluvial environment but consist of sediments that are often deposited rapidly (not allowing sufficient "resetting" of the luminescence signal). In addition they are predominantly high-energy deposits with very few fine-grained intervals, making sampling for OSL difficult.

*2.3.4 Source Rock and Mineralogy*

The thermal history and mineralogy of the regional source rocks can impart a strong influence on the development of luminescence characteristics depending on depositional conditions and the nature of the relevant geologic formations. Photons are accumulated in a mineral by becoming trapped preferentially in defects within its crystal lattice. Therefore, the cooling rate of a respective mineral affects the resulting crystal

structure and consequently the way in which photons are trapped and stored as well as the stability of any luminescence trapped. This is particularly relevant in quartz with regard to the rate and temperature of cooling during crystallization. For example, Sawakuchi et al. (2011) found that metamorphic rocks of higher grade (>500 °C) exhibited more fast OSL component than those formed at a lower metamorphic grade, although they postulated that any effects of the source rock mineralogy might be drowned out by subsequent thermal history and depositional history.

However, Steffen et al. (2009) found that volcanic source rocks can pose significant problems with quartz OSL dating due to an unstable fast component or thermally unstable medium to slow component. It could be that the predominance of unstable OSL components is due to the fast cooling rate of volcanic rocks. Volcanic rocks crystallize more quickly than intrusive or metamorphic rocks, which can cause irregular, unstable crystals to form (Preusser et al., 2006; Rhodes, 2011), which in turn is linked to fading of the regenerative OSL signal.

When fading is seen in feldspars, it is the result of electron trap tunneling and occurs in a pattern that can usually be mathematically accounted for, simply by shifting the growth curve up or down as one unit (Huntley and Lamothe, 2001; Steffen et al., 2009).However, when an unstable fast component is found in quartz, the curve cannot simply be shifted as a unit but instead must be de-convoluted in order to eliminate the unstable component. Since fading can be mathematically accounted for in feldspars, their luminescence, particularly the newest Post-infrared infrared stimulated luminescence (Post-IR-IRSL) may be appropriate to use in a setting such as the Nenana

River Valley. Unfortunately, quartz OSL dating is less versatile, particularly due to the problem of mathematically accounting for unstable and weak component problems.

OSL dating can be quite reliable given the ideal setting, such as a clastic-sourced beach sand (Figure 2.7) that has been extensively reworked allowing the quartz to pass through multiple cycles of irradiation during burial and bleaching. Even within a fluvial environment there is a hierarchy to suitability with sediments further downstream generally having a better OSL signal (strong fast component) due again to an increased amount of reworking and subsequent bleaching (Rhodes, 2011). In terms of source rock, high-grade metamorphism and a slow cooling rate help to form suitable crystals. Crystallization at a high temperature allows the formation of intrinsic point defects which are favored in terms of photon capture (Sawakuchi et al., 2011). However, a slow rate of cooling allows minerals to form lattice free of defects that could cause a thermally unstable crystal to develop.

### *2.3.5 Transport: Fluvial versus Aeolian*

The transport and deposition history of sediment prior to sampling can greatly influence the results of OSL analysis. Aeolian deposits are usually quite suitable as they have generally been fully exposed and reset during the depositional cycle. However, fluvial and glaciofluvial transport processes can be problematic when considering whether to use luminescence techniques, particularly with regard to partial bleaching. Partial bleaching or "incomplete zeroing" is the process by which sediments have not been emptied of their previous luminescence signal during the last erosional path, and

so when re-deposited, they still contain a residual or partial signal that is entirely unrelated to the depositional event the field geologist now wishes to date. Fuchs and Owen (2008) present five scenarios common in glacial environments that are likely to result in partial bleaching; 1) rapid deposition of glacial sediments that limit full exposure to daylight, 2) transport of sediment within or at the base of the glacier, 3) sediment is produced by sub-glacial abrasion with products having never been exposed to daylight prior to deposition, 4) deposited as a "sediment package" with interior portions not exposed to daylight, and 5) deposition that occurs during limited daylight periods at high latitudes (e.g., during the winter months). Furthermore, once this sediment is expunged from the glacier and reworked in the fluvial system, the turbulent fluvial environments which are common to glacially-sourced streams, will limit the amount of additional bleaching for the transported sediments.

## 2.4. Results and Discussion

### *2.4.1 Previous Luminescence Work in central Alaska*

Luminescence dating techniques, including quartz OSL, thermoluminescence (TL), infrared stimulated luminescence (IRSL), and just recently, post-IR IRSL have been applied in central Alaska in both geological and archaeological aspects (Auclair et al., 2007; Berger, 2003; Berger et al., 1994; Dortch, 2006; Dortch et al., 2010; Forgacs, 2013; Johnson et al., 2012; Reuther, 2013; Wygal, 2012). Each specific method has advantages depending on sediment type, depositional environment, and analytical ability. Early methods during the '80s and 90's using TL or IRSL on polymineral fine grains did pay attention to the suitability of quartz OSL, and even once quartz OSL was widely

available, Berger (2003) still utilized both TL and IRSL to determine the chronology of a loess-paleosol and tephra sequence near Fairbanks, Alaska. Berger did report meaningful ages but noted that some TL ages were difficult to interpret. This difficulty could be due to the additional complication for increased partial bleaching characteristics that comes with TL dating.

Problems with quartz OSL dating techniques specifically have been reported in Dortch (2006) and Reuther (2013). Dortch sampled glacial deposits and landforms in the Nenana River valley for both OSL and *in-situ* terrestrial cosmogenic nuclide exposure dating. His cosmogenic exposure dating plan targeted boulders and combined exposure dating and OSL in depth-concentration profiles of terrace deposits. The boulder results largely produced a coherent age sequence for the timing of late Pleistocene glacial advances (Dortch et al., 2010), but the depth-concentration profiles did not produce reasonable ages for the target terraces. The most prominent problems were with the OSL partial bleaching and mixed or reworked sediments.

These issues occurred in tandem because sediment reworking produced a mixture of individual exposure histories as well as complications with partially bleached sediments. The problems with depth concentration profiles were mainly due to shielding related to uneven loess coverage. Dortch et al. (2006) attempted to use the OSL sample ages to calculate this shielding but specific problems associated with OSL data (i.e., reworked sediments, insufficient bleaching, low sensitivity of quartz and variable does rates) made it difficult to obtain accurate values. Reuther (2013) reports

that obtaining reliable results from quartz grains collected in the Nenana valley and surrounding area was not feasible due to dim signals (i.e., lack of fast component).

Reuther attributes the issue with the quartz OSL to proximity to the tectonically active Alaska Range, coupled with poorly suited source rocks and mineral compositions (Reuther, personal communication). Problems with a lack of fast component quartz have also recently been recognized and reported in sediments close to other young, active mountain ranges (Preusser et al., 2006; Tokuyasu et al., 2010; Westaway, 2009). Problems with age underestimation as a result of short depositional history and anomalous fading related to young, active mountain belts has also been noted (Bonde et al., 2001; Preusser et al., 2006; Steffen et al., 2009; Tsukamoto et al., 2007).

In central Alaska, the most success has been achieved with IRSL and Post-IR IRSL techniques. Roberts (2012) and Johnson et al. (2012) recently utilize Post-IR IRSL to date the Old Crow Tephra and vegetated dunes in the Tanana Flats, respectively, and produced results in agreement with independent radiocarbon age control. Forgacs et al. (2013) recently reported anomalously young ages for dunes in the Tanana River lowlands when using both traditional quartz OSL and IRSL techniques. This was chiefly due to problems with fading in the young feldspar, but also potentially due to sediment mixing. They, too, have proposed to utilize Post-IR IRSL as Roberts (2012) did, since this technique can minimize the fading effect in some circumstances.

### *2.4.2 New OSL Results and Interpretation for the Nenana River Valley*

Results of OSL samples taken during the summer of 2012 are presented below (Table 2.2). As can be seen from our decay curves, it was immediately apparent when a sample had a dim signal (Figure 2.3b), was contaminated with feldspars (Figure 2.5b), or did not possess a dominant fast component as demonstrated through falling or rising sensitivity cycles (Figure 2.4b). Almost all of the samples lacked suitable stable components for analysis and the resulting ages are less reliable than we would have suspected when we sampled them. The success of a few of our samples (notably PCS1-OSL and PT2-OSL1 (Figure 2.6a, 2.6b, and 2.6c)) from this batch is almost certainly related to their depositional history.

**TABLE 2.2. QUARTZ OSL DATA AND AGES FOR SAMPLES FROM THE NENANA RIVER VALLEY, AK**

| Sample information | % Water content[a] | K (%)[b] | U (ppm)[b] | Th (ppm)[b] | Cosmic dose[c] (Gy/ka) | Total Dose rate (Gy/ka) | Equivalet dose (Gy) | n[d] | Age (yrs)[e] |
|---|---|---|---|---|---|---|---|---|---|
| **PCS1-OSL** | 4 (42) | 1.70 ± 0.03 | 2.76 ± 0.11 | 10.4 ± 0.26 | 0.21 ± 0.02 | 2.51 ± 0.05 | 31.1 ± 1.83 | 18 (48) | **12,380 ± 770** |
| **PC-OSL3** | 3 (22) | 1.51 ± 0.03 | 2.31 ± 0.13 | 8.27 ± 0.29 | 0.21 ± 0.02 | 2.47 ± 0.07 | 20.3 ± 2.3 | 18 (20) | **8,220 ± 950** |
| **PT2-OSL1** | 9 (28) | 1.64 ± 0.03 | 2.97 ± 0.11 | 9.57 ± 0.26 | 0.22 ± 0.02 | 2.70 ± 0.06 | 14.9 ± 1.00 | 12 (40) | **5,520 ± 400** |
| **SF HFCF-T2-OSL1** | 3 (19) | 1.85 ± 0.06 | 2.95 ± 0.16 | 7.08 ± 0.46 | 0.21 ± 0.02 | 2.89 ± 0.11 | quartz dim | 0 (24) | **no age possible** |
| **SL1-OSL2** | 0 (11) | 1.57± 0.04 | 3.34 ± 0.26 | 11.7 ± 0.33 | 0.22 ± 0.02 | 3.23 ± 0.07 | 23.9 ± 0.98 | 13 (25) | **7,400 ± 340** |
| **SL1-OSL3** | 2 (31) | 1.96 ± 0.03 | 2.44 ± 0.11 | 7.33 ± 0.25 | 0.19 ± 0.01 | 2.64 ± 0.06 | 26.3 ± 2.21 | 15 (35) | **9,850 ± 860** |

| | | | | | | | | | |
|---|---|---|---|---|---|---|---|---|---|
| **SL1-OSL5** | 6 (44) | 1.89 ± 0.03 | 1.93 ± 0.10 | 5.13 ± 0.22 | 0.15 ± 0.01 | 2.13 ± 0.06 | 80.4 ± 4.50 | 12 (20) | **37,750 ± 2,380** |

[a]Field moisture, with figures in parentheses indicating the complete sample saturation %. Ages calculated using approximately 75% of total saturation values.

[b]Analyses obtained using high-resolution lab gamma spectrometry (Ge detector).

[c]Cosmic doses and attenuation with depth were calculated using the methods of Prescott and Hutton (1994). See text for details.

[d]Number of replicated equivalent dose (De) estimates used to calculate the equivalent dose. Figures in parentheses indicate total number of measurements included in calculating the represented equivalent dose and age using radial plots (weighed mean). Dispersion was generally moderate (30%).

[e]Dose rate and age for fine-grained 250-180 microns sized quartz. Exponential + linear fit used on equivalent dose, errors to one sigma.

We have chosen three samples to discuss, one that produced satisfactory results and two that proved problematic. The worst sample for quartz OSL was SFHCF-T2-OSL. The source rock for this sample is metamorphic and mainly made up of quartz with minor amounts of Na-plagioclase, but it clearly lacks a fast component and emits a dim signal (Figure 2.3a, 2.3b, and 2.3c). Even when the quartz produced a stronger signal, the sensitivity cycles were still falling rather precipitously (Figure 2.4a, 2.4b, and 2.4c). Because of these characteristics we were not able to obtain an age from it all (Table 2.2). This sample was taken in a paleoseismic trench with the purpose of constraining neotectonic activity. Although it was taken from what looked to be a suitable fine-grained fluvial deposit, the erosional history of this deposit is likely problematic. For example, this sample is located farthest upstream, and the sample site is located near two smaller tributary drainages, as well being the most proximal to a glacier of any of our samples.

Sample PC-OSL3b was taken from a sandy fluvial terrace riser deposit (Fig 2.2 & 2.5, Table 2.2) and yielded an OSL age of 8,220 ± 950 yrs (Table 2.2). Mineralogically it is made up of quartz, microcline, and albite, with small, dark (< 60 microns) grains identified as garnets and biotites indicating biotite-rich phyllite and schist as a source

rock. This sample was taken in what is likely a remnant outwash terrace from the Carlo glaciation, although it has been mapped as Riley Creek (Dortch et al., 2010). However, previous work on the Riley Creek glaciation has estimated a range of 8-61 ka (Dortch et al., 2010) and Dortch's study produced ages of 22-30 ka for these landforms. After digesting the results from this sample, we can show that analytically it was not ideal (Fig 2.5a, 2.5b, 2.5c), and may have been contaminated with plagioclase or quartz with plagioclase inclusions from the metamorphic source geology. The results of PC-S1 can likely be interpreted in a similar manner since it was taken stratigraphically below PC-OSL3b (0.5m) in in the same location. This sample produced an OSL age of 12,380 ±770 yrs. Although this is good relative to PC-OSL3b we are still not confident in these results since it was taken in the same deposit as PC-OSL3b. This sample was taken in a terrace-capping loess deposit so our results do make sense.

Sample PT2-OSL1, which analytically produced the most satisfactory results, exhibited optimum regeneration and a good OSL fast component (Figure 2.6a, 2.6b, and 2.6c). This sample was taken within what is thought to be the same age fluvial sand deposits as PC-OSL3b, but produced a younger age (5,520 ± 400 yrs; Table 8). However, we are more confident about this sample for two reasons; 1) the analytical behavior of the sample and 2) recent, independent age control taken in the same section. This age control was a radiocarbon sample taken lower in the strata, which produced an age of 7,594-7,965 Cal BP. These two facts alone give us confidence that this result is quite accurate and can be trusted. The suitability of this sample is likely due to its position (i.e., furthest down the drainage), which suggests that the sediment has gone through

sufficient cycles of repeated erosion and burial to completely bleach and reset the luminescence signal. The source geology of this sample is similar to the others.

The SL-series samples (taken at the Slate Creek site, Figure 2.2), produced curious results. The deposit is of Lignite Creek age (approximately 130-200 ka) but the two upper deposits analyzed (SL1-OSL2, SL1-OSL3), were from younger terrace capping loess. These two samples produced OSL ages of 7,400 ± 340 and 9,850 ± 860 yrs, respectively, which could be potentially accurate for loess depositional ages on this landform. However, the stratigraphically lowest sample analyzed (SL1-OSL5) produced an age of 37,750 ± 2,380 yrs, which is much younger than expected. This site requires further interpretation to assess the validity of our results.

*2.4.3 Example Decay and Growth Curves*

Figures 2.3b, 2.3c; 2.4b, 2.4c, 2.5b, 2.5c, 2.6b, and 2.6c) are decay and growth curves that show an example of our varied results. OSL decay curves show quartz signal for each sample measured as a continuous wave. The x-axis is time of measurement in seconds (s) and the y-axis is photon counts/second over the course of the 40s. PT2-OSL1 (Figure 2.6b) shows a sharp decay after 1-2 seconds indicating access from a fast OSL component. Figure 2.5b, shows a decay that is not as sharp and continues with a generally elevated base throughout. This behavior indicates a weak fast component signal or feldspar contamination. Figures 2.3b and 2.4b illustrate the generally unacceptable decay curves of our worst behaved sample.

OSL growth curves for each sample shows the natural signal (red lines) plotted on the Lx/Tx axis above 1.0. The x-axis is the equivalent dose measured in Grays (source calibration is 0.081 Gy/sec. The bleach (zero) is shown at the junction of the axes. The y-axis shows luminescence response over the test dose response (Lx/Tx or unitless normalized OSL sensitivity measurements). PT2-OSL1 (Figure 2.6c) exhibits optimal regeneration with a recycle within 1% of the first measurement (two clustered circles close to the 1.0 x-axis mark. PC-OSL3b (Figure 2.5c) does not exhibit “optimal” regeneration. Both Figure 2.3c and 2.4c demonstrate dim signals, large errors, and falling ratios, indicating the general unsuitability of this sample for quartz OSL.

*2.4.4 Decision Tree*

As stated earlier, many researchers have offered protocols and experiments designed to aid the field geologist in obtaining the most reliable quartz OSL ages (review in Wintle (2010). Our aim is to aid the researcher in the field as they collect, before ever getting the sample to the OSL laboratory, by taking previous research, adding that to our experiments, and then offering a decision-tree process whereby the field geologist can ascertain where best to sample (Figure 2.7).

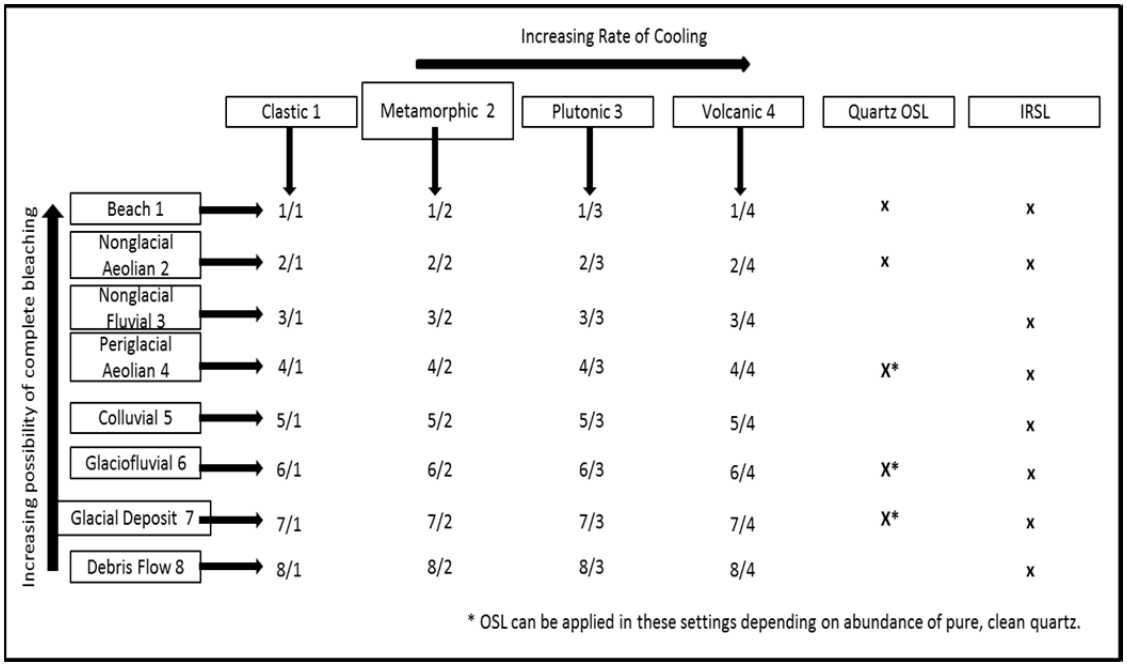


**Figure 2.7: Decision-tree for luminescence sampling.** This chart is intended to aid the researcher in determining the suitability of sediments to luminescence sampling and is based on depositional history and source rock cooling rate. Deposit types are listed on the left hand side in order of increasing possibility of complete bleaching (1-8, with 1 being well-bleached and 8 least bleached). Four main classes of possible source rocks are listed on the top; clastic, metamorphic, plutonic, and volcanic (1-4). The metamorphic, plutonic, and volcanic rocks are listed from left to right in order of decreasing rate of cooling (i.e., metamorphic has the lowest cooling rate and volcanic the highest). The two columns on the right indicate suggested luminescence to apply in a particular setting. Deposit type is listed first, i.e. a "1/1" indicates a clastic beach setting and is the most desirable and an "8/4" indicates a volcanic debris flow and is the least desirable. Adapted from Rhodes, 2011 (his Figure 7).

The importance of knowing your source rock when applying OSL dating techniques has been addressed for other regions (Preusser et al., 2006), but not specifically in Alaska. However, Sawakuchi et al. (2011) argue that source rock has little effect on luminescence sensitivity, but instead thermal regime and depositional history are the main factors. Sawakuchi et al.(2011) state that in their study rocks with a cooling temperature of >500 °C showed the best fast component of quartz due to the concentration of Si and O vacancies (intrinsic point defects) as well as increased $Si^{4+}$ and $Al^{3+}$ substitutions which create luminescence-trapping defects in quartz. We argue that although cooling temperature and depositional history do play a large role in quartz sensitivity (for example, SFHCF-T2-OSL and PC-OSL3b), the rate of cooling is also important because of the effects it seems to have on crystal structure and subsequent thermal stability. When a rock cools quickly the crystal lattice of minerals within do not develop into clean complete crystals but rather into an irregular "leaky" lattice and electron trap tunneling can occur (Rhodes, 2011). Later on when these grains are being transported and exposed to light the lattice cannot capture (and retain) photons to its full capacity, leading to a lack of a fast component and can cause a significant underestimation of age (Preusser et al., 2009).

Understanding the mineralogical composition of your chosen study area is an important factor to consider in order to obtain reliable data. Ridgway et al. (2007) reported mineralogical composition of the Usibelli Group to be 42.67% lithics, with 54.80% of this percentage being volcanic in the Nenana Gravel, and only 36.68% quartz and 18.65% feldspar. This report provides insight into the details of sediment

composition for one formation in our study area; however, the Usibelli Group is only one of several formations making up the source rock of the Nenana River including the Birch Creek Schist, Totatlanika Schist, Cantwell Formation, Kahiltna Assemblage, and the Teklanika Formation. Further mineralogical surveys are necessary in this region to complete the picture and constrain the reliability of luminescence dating techniques.

Since the majority of sediment supplying the Nenana River is sourced from metamorphic and plutonic rocks, and thus should provide amenable source geology for OSL, we have concluded that our mixed success with OSL samples is mainly due to the poor erosional and depositional history. However, source rock can still affect OSL suitability and regions with volcanic source rocks should be avoided.

**2.5. Conclusion**

The aim of this chapter has been to address the importance of obtaining a full understanding of the depositional history and source rock of your sediment prior to ever going into the field. Although it appears from our study that very short and infrequent erosional events actually control the majority of the poor OSL characteristics, we cannot completely discount the mixture of differing geologic terranes within the unconsolidated sediment. These factors are crucial to obtaining reliable, meaningful results so we have included a decision tree process along with a discussion of suitability of material typically available to the researcher. It is our hope that this research will compliment previous research (reviewed in Wintle et al., 2010) by providing a more complete toolset for researchers interested in utilizing luminescence dating techniques.

While the young tectonics coupled with glacial sediment of the Nenana River valley makes it less than ideal for the application of quartz OSL; IRSL, TL, and Post-IR IRSL have been used with limited documented success (e.g., Reuther 2013; Berger 2003; Berger 1994; AuClair et al. 2007; Forgacs et al. 2013; Johnson et al. 2012; Roberts 2012; and Wygal and Goebel 2012). Post IR-IRSL shows a promising future application of this technique, but it is yet to be tested in tectonically active areas. Since the majority of sediment supplying the Nenana River is sourced from metamorphic and plutonic rocks and thus should be producing good quality quartz for OSL dating, we have concluded that our mixed success with OSL samples is mainly due to a poor erosional and depositional history and not the source rock itself. However, source rock can still dominate OSL suitability especially in regions with volcanic source rocks and these should be avoided when possible. The decision tree we have modifed is a reliable and accessible way to not only understand the important aspects of OSL application but a convenient way to plan for the best possible results with nothing but a geologic map, before even collecting your sample.

# Appendix A: *k* Calculation Data

| ID | MP x | MP y | tan θ | area ($m^2$) | angle | age | age error | $q_s$ ($m^2$/year) | $S_c$ | k ($m^2$/year) |
|---|---|---|---|---|---|---|---|---|---|---|
| CAE1 | 124.85 | 310.9 | 0.162 | 4.87 | 9.2 | 18000 | 2000 | 0.00027 | 0.71 | 0.005548848 |
| CAE2 | 109.1 | 311.5 | 0.17 | 9.09 | 9.65 | 18000 | 2000 | 0.00051 | 0.71 | 0.0028841 |
| CAE3 | 150.5 | 314.65 | 0.25 | 14.097 | 14 | 18000 | 2000 | 0.00078 | 0.71 | 0.00139685 |
| CAE4 | 101.3 | 312.7 | 0.216 | 23.97 | 12.2 | 18000 | 2000 | 0.00133 | 0.71 | 0.00103977 |
| CAE5 | 130.63 | 312.37 | 0.2595 | 14.126 | 16.9 | 18000 | 2000 | 0.00078 | 0.71 | 0.002903771 |
| CAE6 | 91.41 | 312.52 | 0.2095 | 20.65 | 11.8 | 18000 | 2000 | 0.00115 | 0.71 | 0.001240094 |
| CAW12 | 81.105 | 244.8 | 0.233 | 28.29 | 13.1 | 18000 | 2000 | 0.00157 | 0.71 | 0.023852375 |
| CAW3 | 84.2 | 237.6 | 0.22 | 5.95 | 12.4 | 18000 | 2000 | 0.00033 | 0.71 | 0.009380296 |
| CAW4 | 85.31 | 237.4 | 0.213 | 5.89 | 12 | 18000 | 2000 | 0.00033 | 0.71 | 0.020756149 |
| CAW5 | 81.38 | 237.5 | 0.177 | 9.2 | 10 | 18000 | 2000 | 0.00051 | 0.71 | 0.016983772 |
| CAW7 | 63.02 | 238.6 | 0.131 | 11.76 | 7.5 | 18000 | 2000 | 0.00065 | 0.71 | 0.017936735 |
| CAW11 | 62.61 | 242.68 | 0.226 | 13.9 | 12.7 | 18000 | 2000 | 0.00077 | 0.71 | 0.029747308 |
| RCE1 | 180.0537 | 243.3 | 0.364 | 46.18 | 20 | 25000 | 3000 | 0.00185 | 0.71 | 0.001583149 |
| RCE2 | 162.3858 | 242.96 | 0.358 | 47.2 | 19.7 | 25000 | 3000 | 0.00189 | 0.71 | 0.002800285 |
| RCE3 | 132.3681 | 241.06 | 0.487 | 24.29 | 25.9 | 25000 | 3000 | 0.00097 | 0.71 | 0.002744268 |
| RCE4 | 131.5109 | 243.9 | 0.497 | 26.74 | 26.4 | 25000 | 3000 | 0.00107 | 0.71 | 0.005594522 |
| RCE5 | 149.7692 | 244.5 | 0.526 | 22.6 | 27.8 | 25000 | 3000 | 0.00090 | 0.71 | 0.002620205 |
| RCE6 | 141.7169 | 244.7 | 0.444 | 34.37 | 23.9 | 25000 | 3000 | 0.00137 | 0.71 | 0.004999225 |
| RCW1 | 100.1687 | 275.8 | 0.23 | 4.85 | 13 | 25000 | 3000 | 0.00019 | 0.71 | 0.006018911 |
| RCW2 | 100.5956 | 275.7 | 0.2 | 2.07 | 11.3 | 25000 | 3000 | 0.00008 | 0.71 | 0.001358264 |
| RCW3 | 100.0648 | 275.8 | 0.225 | 6.685 | 13 | 25000 | 3000 | 0.00027 | 0.71 | 0.001397992 |
| RCW4 | 99.8657 | 275.82 | 0.23 | 0.67 | 12.95 | 25000 | 3000 | 0.00003 | 0.71 | 0.002708172 |
| RCW5 | 101.9533 | 269.1 | 0.234 | 5.635 | 13.7 | 25000 | 3000 | 0.00023 | 0.71 | 0.004817496 |
| RCW6 | 100.2979 | 275.8 | 0.223 | 6.72 | 12.5 | 25000 | 3000 | 0.00027 | 0.71 | 0.003070707 |
| HEW1 | 155.69 | 325.34 | 0.096 | 0.9763 | 5.5 | 60000 | 4000 | 0.00002 | 0.71 | 0.003740901 |
| HEW2 | 173.06 | 325.58 | 0.235 | 3.254 | 13.2 | 60000 | 4000 | 0.00005 | 0.71 | 0.00393293 |
| HEW3 | 179 | 325.19 | 0.1275 | 18.41 | 7.3 | 60000 | 4000 | 0.00031 | 0.71 | 0.00105643 |
| HEW5 | 187.84 | 327.1 | 0.645 | 4.06 | 32.8 | 60000 | 4000 | 0.00007 | 0.71 | 0.001097577 |
| HEW6 | 206.02 | 328.32 | 0.077 | 31.697 | 4.4 | 60000 | 4000 | 0.00053 | 0.71 | 0.000775358 |
| HEW9 | 157.21 | 330.591 | 0.065 | 12.347 | 3.7 | 60000 | 4000 | 0.00021 | 0.71 | 0.001885503 |

| | | | | | | | | | | |
|---|---|---|---|---|---|---|---|---|---|---|
| HEE1 | 249.2462 | 321.44581 | 0.0956 | 8.8513 | 5.46 | 60000 | 4000 | 0.00015 | 0.71 | 0.000754964 |
| HEE2 | 272.7692 | 321.74862 | 0.222 | 3.827059 | 12.52 | 60000 | 4000 | 0.00006 | 0.71 | 0.000381149 |
| HEE3 | 265.6127 | 322.50136 | 0.192 | 26.71 | 10.9 | 60000 | 4000 | 0.00045 | 0.71 | 0.001069093 |
| HEE4 | 183.1149 | 330.68482 | 0.1642 | 26.22 | 9.3 | 60000 | 4000 | 0.00044 | 0.71 | 0.000104294 |
| HEE5 | 300.3429 | 322.6 | 0.108 | 18.01232 | 6.16 | 60000 | 4000 | 0.00030 | 0.71 | 0.000858619 |
| HEE6 | 247.0155 | 407.45 | 0.075 | 26.04832 | 4.29 | 60000 | 4000 | 0.00043 | 0.71 | 0.001086471 |
| **LiDAR** | **LiDAR** | **LiDAR** | **LiDAR** | **LiDAR** | **LiDAR** | **LiDAR** | **LiDAR** | **LiDAR** | **LiDAR** | **LiDAR** |
| CAWL1 | 47.4954 | 293.148 | 0.234 | 12.3012 | 13.17 | 18000 | 4000 | 0.00068 | 0.71 | 0.002603283 |
| CAWL2 | 38.7149 | 294.556 | 0.2755 | 10.0686 | 15.4 | 18000 | 4000 | 0.00056 | 0.71 | 0.001724665 |
| CAWL3 | 42.5122 | 293.325 | 0.2731 | 13.753 | 15.275 | 18000 | 4000 | 0.00076 | 0.71 | 0.002383781 |
| CAWL4 | 45.4451 | 293.516 | 0.29265 | 13.2291 | 16.312 | 18000 | 4000 | 0.00073 | 0.71 | 0.002084694 |
| CAWL5 | 48.3941 | 293.676 | 0.2991 | 12.1939 | 16.652 | 18000 | 4000 | 0.00068 | 0.71 | 0.001862976 |
| CAWL6 | 60.6362 | 293.301 | 0.28865 | 9.90134 | 16.1 | 18000 | 4000 | 0.00055 | 0.71 | 0.001590705 |

## Appendix B: XRD Data

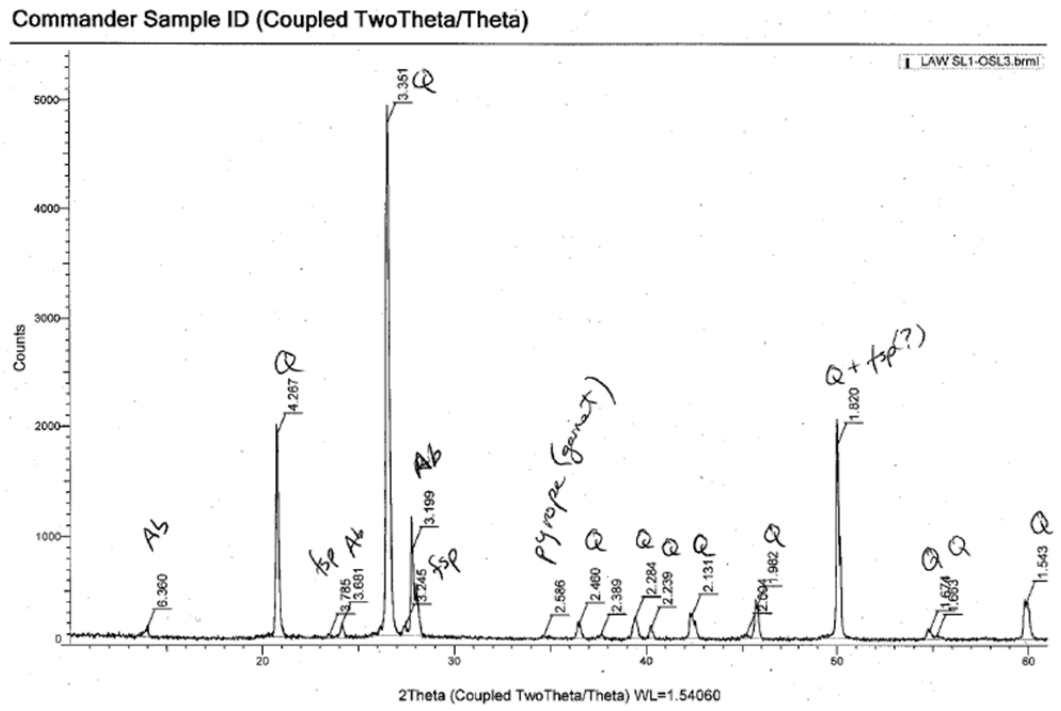


**Sample SL1-OSL3:** Quartz, pyrope garnet, albite feldspar, possible microcline feldspar

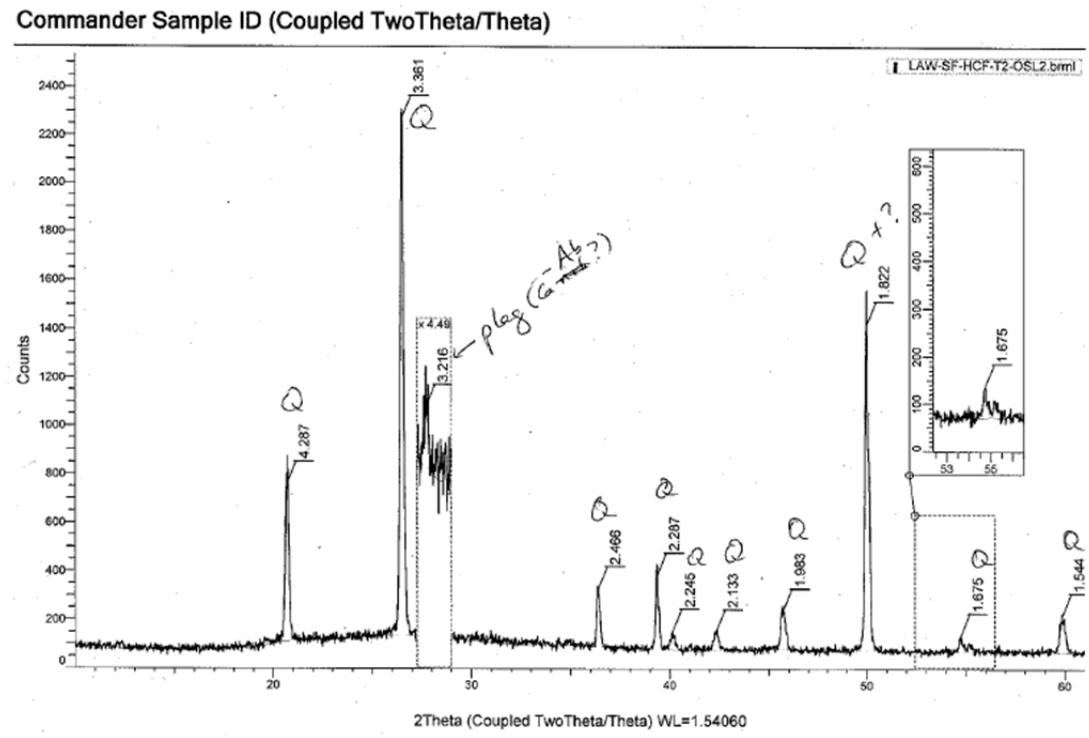


**Sample: SF-HCF-T2-OSL2.** Quartz with very minor Na-plagioclase.

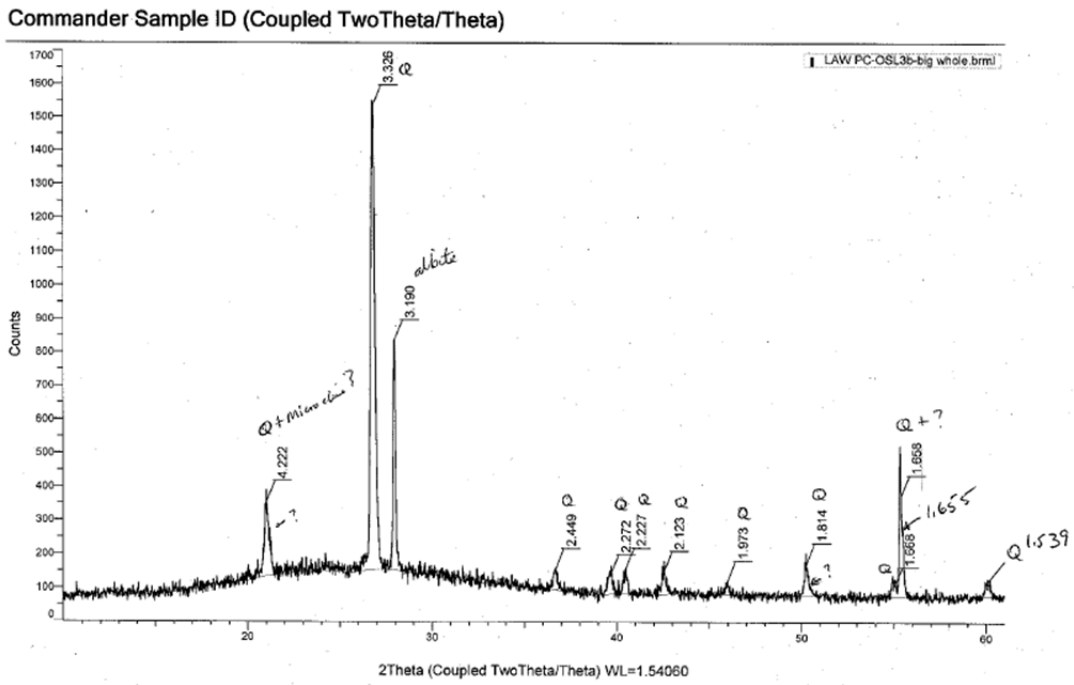


**Sample PC-OSL3**: Quartz, microcline, albite. Source: granite or granitic gneiss

## References


Anthony, K. M. W., Anthony, P., Grosse, G., and Chanton, J., 2012, Geologic methane seeps along boundaries of Arctic permafrost thaw and melting glaciers: Nature Geoscience, v. 5, no. 6, p. 419-426.

Auclair, M., Lamothe, M., Lagroix, F., and Banerjee, S. K., 2007, Luminescence investigation of loess and tephra from Halfway House section, Central Alaska: Quaternary Geochronology, v. 2, no. 1, p. 34-38.

Begét, J. E., Stone, D. B., and Hawkins, D. B., 1990, Paleoclimatic forcing of magnetic susceptibility variations in Alaskan loess during the late Quaternary: Geology, v. 18, no. 1, p. 40-43.

Bemis, S. P., 2010, Moletrack scarps to mountains: Quaternary tectonics of the central Alaska Range [PhD: University of Oregon, 121 p.

Bemis, S. P., Carver, G. A., and Koehler, R. D., 2012, The Quaternary thrust system of the northern Alaska Range: Geosphere, v. 8, no. 1, p. 196-205.

Bemis, S. P., and Wallace, W. K., 2007, Neotectonic framework of the north-central Alaska Range foothills: Geological Society of America Special Papers, v. 431, p. 549-572.

Berger, G. W., 2003, Luminescence chronology of late Pleistocene loess-paleosol and tephra sequences near Fairbanks, Alaska: Quaternary Research, v. 60, no. 1, p. 70-83.

Berger, G. W., Pillans, B. J., and Palmer, A. S., 1994, Test of thermoluminescence dating of loess from New Zealand and Alaska: Quaternary Science Reviews, v. 13, no. 4, p. 309-333.

Bonan, G. B., 1989, A computer model of the solar radiation, soil moisture, and soil thermal regimes in boreal forests: Ecological Modelling, v. 45, no. 4, p. 275-306.

Bonde, A., Murray, A., and Friedrich, W. L., 2001, Santorini: Luminescence dating of a volcanic province using quartz?: Quaternary Science Reviews, v. 20, no. 5–9, p. 789-793.

Brennan, P. R., Gilbert, H., and Ridgway, K. D., 2011, Crustal structure across the central Alaska Range: Anatomy of a Mesozoic collisional zone: Geochemistry, Geophysics, Geosystems, v. 12, no. 4.

Briner, J. P., and Kaufman, D. S., 2008, Late Pleistocene mountain glaciation in Alaska: key chronologies: Journal of Quaternary Science, v. 23, no. 6-7, p. 659-670.

Chapin, F. S., Oswood, M. W., Van Cleve, K., Viereck, L. A., Verbyla, D. L., and Chapin, M. C., 2006, Alaska's changing boreal forest, Oxford University Press New York.

Clarke, B. A., and Burbank, D. W., 2010, Evaluating hillslope diffusion and terrace riser degradation in New Zealand and Idaho: Journal of Geophysical Research: Earth Surface, v. 115, no. F2, p. F02013.

Csejtey, B., J.r, Mullen, M.W., Cox, D.P., and Stricker, G.D., 1992, Geology and Geochronology of the Healy quadrangle, South-Central Alaska: USGS, US Geological Survey Miscellaneous Investigations Series Map, scale 1:250,000.

Culling, W. E. H., 1960, Analytical Theory of Erosion: The Journal of Geology, v. 68, no. 3, p. 336-344.

Ding, Z., Sun, J., Rutter, N. W., Rokosh, D., and Liu, T., 1999, Changes in Sand Content of Loess Deposits along a North–South Transect of the Chinese Loess Plateau and the Implications for Desert Variations: Quaternary Research, v. 52, no. 1, p. 56-62.

Dortch, J., 2006, Defining the timing of glaciation in the central Alaska Range using terrestrial cosmogenic nuclide and optically stimulated luminescence dating of moraines and terraces: Master's thesis, University of Cincinnati.

Dortch, J. M., Owen, L. A., Caffee, M. W., Li, D., and Lowell, T. V., 2010, Beryllium-10 surface exposure dating of glacial successions in the Central Alaska Range: Journal of Quaternary Science, v. 25, no. 8, p. 1259-1269.

Dowman, I., 2004, Integration of LIDAR and IFSAR for mapping: International Archives of Photogrammetry and Remote Sensing, v. 35, no. B2, p. 90-100.

Duller, G. A., 2008, Single-grain optical dating of Quaternary sediments: why aliquot size matters in luminescence dating: Boreas, v. 37, no. 4, p. 589-612.

Durcan, J. A., and Duller, G. A., 2011, The fast ratio: a rapid measure for testing the dominance of the fast component in the initial OSL signal from quartz: Radiation Measurements, v. 46, no. 10, p. 1065-1072.

Dusel-Bacon, C., Wooden, J. L., and Hopkins, M. J., 2004, U-Pb zircon and geochemical evidence for bimodal mid-Paleozoic magmatism and syngenetic base-metal mineralization in the Yukon-Tanana terrane, Alaska: Geological Society of America Bulletin, v. 116, no. 7-8, p. 989-1015.

Eberhart-Phillips, D., Christensen, D. H., Brocher, T. M., Hansen, R., Ruppert, N. A., Haeussler, P. J., and Abers, G. A., 2006, Imaging the transition from Aleutian subduction to Yakutat collision in central Alaska, with local earthquakes and active source data: Journal of Geophysical Research: Solid Earth, v. 111, no. B11, p. B11303.

Edwards, M., and Armbruster, W., 1989, A tundra-steppe transition on Kathul Mountain, Alaska, USA: Arctic and Alpine Research, p. 296-304.

Fathai, M. a. S., S., 2003, Dating volcanic and related sediments by luminescence methods: a review: Earth Science Reviews, v. 62, p. 229-264.

Forgacs, C. A., IRSL Dating of a vegetated dune field in central Alaska, *in* Proceedings Geological Society of America Abstracts with Programs2013, Volume 45, p. 0.

Fuchs, M., and Owen, L. A., 2008, Luminescence dating of glacial and associated sediments: review, recommendations and future directions: Boreas, v. 37, no. 4, p. 636-659.

Hanks, T. C., 2000, The age of scarplike landforms from diffusion-equation analysis: Quaternary Geochronology: Methods and Applications, p. 313-338.

Hsu, L., and Pelletier, J. D., 2004, Correlation and dating of Quaternary alluvial-fan surfaces using scarp diffusion: Geomorphology, v. 60, no. 3, p. 319-335.

Huntley, D. J., and Lamothe, M., 2001, Ubiquity of anomalous fading in K-feldspars and the measurement and correction for it in optical dating: Canadian Journal of Earth Sciences, v. 38, no. 7, p. 1093-1106.

Johnson, W. C., Gaines, E. P., Halfen, A. F., Hanson, P. R., and Young, A. R., Role of Dune Landscape Development in Determining Cultural Foci within the Tanana Flats, Central Alaska, *in* Proceedings 2012 GSA Annual Meeting in Charlotte2012.

Molnar, P., Brown, E. T., Burchfiel, B. C., Deng, Q., Feng, X., Li, J., Raisbeck, G. M., Shi, J., Zhangming, W., and Yiou, F., 1994, Quaternary climate change and the formation of river terraces across growing anticlines on the north flank of the Tien Shan, China: The Journal of Geology, p. 583-602.

Muhs, D. R., Ager, T. A., Been, J., Bradbury, J. P., and Dean, W. E., 2003, A late Quaternary record of eolian silt deposition in a maar lake, St. Michael Island, western Alaska: Quaternary Research, v. 60, no. 1, p. 110-122.

Muhs, D. R., Ager, T. A., and Begét, J. E., 2001, Vegetation and paleoclimate of the last interglacial period, central Alaska: Quaternary Science Reviews, v. 20, no. 1, p. 41-61.

Muhs, D. R., Ager, T.A., Bettis III, E., McGeehin, J., Been, J.M., Beget, J.E., Pavich, M.J., Stafford, Jr., T.W., and Stevens, De Anne S.P., 2001, Stratigraphy and paleoclimate significance of Late Quaternary loess-paleosol sequences of the Late interglacial-Glacial cycle in central Alaska *in* USGS, ed.

Nash, D. B., 1984, Morphologic dating of fluvial terrace scarps and fault scarps near West Yellowstone, Montana: Geological Society of America Bulletin, v. 95, no. 12, p. 1413-1424.

Pewe, T. L., 1955, Origin of the upland silt near Fairbanks, Alaska: Geological Society of America Bulletin, v. 66, no. 6, p. 699-724.

Péwé, T. L., 1975a, Quaternary geology of Alaska, US Government Printing Office.

-, 1975b, Quaternary stratigraphic nomenclature in unglaciated central Alaska, US Government Printing Office.

Péwé, T. L., Wahrhaftig, C., Weber, F.R., 1966, Geologic map of the Fairbanks quadrangle, Alaska, USGS.

Preusser, F., Chithambo, M. L., Götte, T., Martini, M., Ramseyer, K., Sendezera, E. J., Susino, G. J., and Wintle, A. G., 2009, Quartz as a natural luminescence dosimeter: Earth-Science Reviews, v. 97, no. 1–4, p. 184-214.

Preusser, F., Ramseyer, K., and Schlüchter, C., 2006, Characterisation of low OSL intensity quartz from the New Zealand Alps: Radiation Measurements, v. 41, no. 7–8, p. 871-877.

Reuther, J. D., 2013, Late Glacial and Early Holocene Geoarchaeology and Terrestrial Paleoecology in the Lowlands of the Middle Tanana Valley, Subarctic Alaska.

Rhodes, E. J., 2011, Optically stimulated luminescence dating of sediments over the past 200,000 years: Annual Review of Earth and Planetary Sciences, v. 39, p. 461-488.

Ridgway, K. D., Thoms, E. E., Layer, P. W., Lesh, M. E., White, J. M., and Smith, S. V., 2007, Neogene transpressional foreland basin development on the north side of the central Alaska Range, Usibelli Group and Nenana Gravel, Tanana basin: Geological Society of America Special Papers, v. 431, p. 507-547.

Roberts, H. M., 2012, Testing Post-IRL IRSL protocols for minimzing fading in feldspars, using Alaskan loess with independent chronolgical control: Radiation Measurements, v. 47, no. 9, p. 716-724.

Roering, J. J., Kirchner, J. W., and Dietrich, W. E., 1999, Evidence for nonlinear, diffusive sediment transport on hillslopes and implications for landscape morphology: Water Resources Research, v. 35, no. 3, p. 853-870.

Rowland, J., Jones, C., Altmann, G., Bryan, R., Crosby, B., Hinzman, L., Kane, D., Lawrence, D., Mancino, A., and Marsh, P., 2010, Arctic landscapes in transition: responses to thawing permafrost: Eos, Transactions American Geophysical Union, v. 91, no. 26, p. 229-230.

Sawakuchi, A. O., Blair, M. W., DeWitt, R., Faleiros, F. M., Hyppolito, T., and Guedes, C. C. F., 2011, Thermal history versus sedimentary history: OSL sensitivity of quartz grains extracted from rocks and sediments: Quaternary Geochronology, v. 6, no. 2, p. 261-272.

Slatton, K. C., and Carter, W. E., 2008, A Primer for Airborne Lidar.

Steffen, D., Preusser, F., and Schlunegger, F., 2009, OSL quartz age underestimation due to unstable signal components: Quaternary Geochronology, v. 4, no. 5, p. 353-362.

Ten Brink, N. W., and Waythomas, C.F., 1985, Late Wisconsin glacial chronology of the north-central Alaska Range: A regional synthesis and its implications for early human settlements: National Geographic Society.

Thoms, E. E., 2000, Late Cenozoic unroofing sequence and foreland basin development of the central Alaska Range: implications from the Nenana Gravel: University of Alaska Fairbanks.

Thorson, R. M., and Bender, G., 1985, Eolian deflation by ancient katabatic winds: a late Quaternary example from the north Alaska Range: Geological Society of America Bulletin, v. 96, no. 6, p. 702-709.

Tokuyasu, K., Tanaka, K., Tsukamoto, S., and Murray, A., 2010, The characteristics of OSL signal from quartz grains extracted from modern sediments in Japan: Geochronometria, v. 37, no. 1, p. 13-19.

Tsukamoto, S., Murray, A. S., Huot, S., Watanuki, T., Denby, P. M., and Bøtter-Jensen, L., 2007, Luminescence property of volcanic quartz and the use of red isothermal TL for dating tephras: Radiation Measurements, v. 42, no. 2, p. 190-197.

Viereck, L., 2010, Alaska trees and shrubs, University of Alaska Press.

Wahrhaftig, C., 1968, Schists of the central Alaska Range, US Government Printing Office.

Wahrhaftig, C. a. B., R.F., 1958, Engineering geology along part of the Alaska Railroad, U.S. Geological Survey, p. 79-118.

Westaway, K., 2009, The red, white and blue of quartz luminescence: A comparison of $D_e$ values derived for sediments from Australia and Indonesia using thermoluminescence and optically stimulated luminescence emissions: Radiation Measurements, v. 44, no. 5, p. 462-466.

Westgate, J. A., Stemper, B. A., and Péwé, T. L., 1990, A 3 my record of Pliocene-Pleistocene loess in, interior Alaska: Geology, v. 18, no. 9, p. 858-861.

Wintle, A. G., 2010, Future directions of luminescence dating of quartz: Geochronometria, v. 37, no. 1, p. 1-7.

Wintle, A. G., and Murray, A. S., 2006, A review of quartz optically stimulated luminescence characteristics and their relevance in single-aliquot regeneration dating protocols: Radiation Measurements, v. 41, no. 4, p. 369-391.

Wygal, B. T., and Goebel, T., 2012, Early Prehistoric archaeology of the Middle Susitna valley, Alaska: Arctic Archaeology, v. 49, no. 1, p. 45-67.

Zheng, C. X., Zhou, L. P., and Qin, J. T., 2009, Difference in luminescence sensitivity of coarse-grained quartz from deserts of northern China: Radiation Measurements, v. 44, no. 5–6, p. 534-537.

## Vita

**Place of Birth:** Rhinebeck, NY, USA

**Educational Institutions and Degrees Already Awarded:** Vassar College, B.A. in Earth Science, 2011.

**Professional Positions Held:** Graduate Research Assistant, Graduate Teaching Assistant, Estuary Research Intern, Environmental Educator, Naturalist, Veterinary Assistant

**Scholastic and Professional Honors:** Outstanding Teaching Assistant Award, Helen Miringoff Award for outstanding performance in fieldwork

**Professional Publications:**

Bemis, S.P., DeVore, J.R., Federschmidt, S., Taylor, T.P., and **Walker, L.A.** Synthesis of results from a transect of paleoseismic investigations across the Alaska Range, Abstract for 2014 SSA Meeting, April 30-May 2, Anchorage, AK.

**Walker, L.A.**, Mahan, S.A., Bemis, S.P. Effects of depositional history and provenance on quartz luminescence dating: a case study in the Nenana River Valley, central Alaska, *Quaternary International Special Issue: 9$^{th}$ New World Luminescence Workshop,* In Review.

DeVore, J.R., **Walker, L.A**., Bemis, S.P., Quaternary geologic map of the northern Healy B4 quadrangle, Alaska – Denali fault tectonic geomorphology and Nenana River incision history, In preparation.

**Walker, L.A.**, Bemis, S.P., and DeVore, J.R., 2013, The effects of global climate change on landscape evolution in the boreal forest of the central Alaska Range, poster, GSA Abstracts and Programs v.45, n.7, Ref: Abstract No: 227630

Bemis, S.P., **Walker, L.A**., Burkett, C., and DeVore, J.R**.,** 2013, Use of 3D models derived from handheld photography in paleoseismology, Digital Poster, GSA Abstracts with Program, v. 45, n.7, Ref: Abstract No: 233688

DeVore, J.R., Bemis, S.P., and **Walker, L.A.,** 2012, Evidence for post-26 ka displacement of the Northern Foothills thrust at the Nenana River, Alaska: Eos (Transactions of the American Geophysical Union), Abstract T11A-2552.

**Walker, L.A.,** 2009, The Eel Project, Dutchess Watershed Webpage, http://www.dutchesswatersheds.org/research/175-the-eel-project

Vojnovic, Igor, ed. 2011. Favelas, Urban Renewal, and Guanabara Bay: Environmental justice and Sustainability in Rio de Janeiro," in *Sustainability: A Global Urban Context.* Michigan State University Press. (Maps made by **Laurel Walker**)

**Student Full Name:** Laurel Anne Walker